



Universiteit Gent  
Faculteit Wetenschappen  
Vakgroep Fysica en Sterrenkunde

<sup>2</sup> No title yet

<sup>3</sup> No sub-title neither, obviously...

---

<sup>4</sup> Alexis Fagot

5



Thesis to obtain the degree of  
Doctor of Philosophy in Physics  
Academic years 2012-2017







Universiteit Gent  
Faculteit Wetenschappen  
Vakgroep Fysica en Sterrenkunde

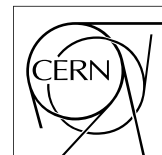
Promotoren: Dr. Michael Tytgat  
Prof. Dr. Dirk Ryckbosch

Universiteit Gent  
Faculteit Wetenschappen  
Vakgroep Fysica en Sterrenkunde  
Proeftuinstraat 86, B-9000 Gent, België  
Tel.: +32 9 264.65.28  
Fax.: +32 9 264.66.97

17



Thesis to obtain the degree of  
Doctor of Philosophy in Physics  
Academic years 2012-2017





## Acknowledgements

<sup>19</sup> Ici on remerciera tous les gens que j'ai pu croiser durant cette aventure et qui m'ont permis de passer  
<sup>20</sup> un bon moment

<sup>21</sup> *Gent, ici la super date de la mort qui tue de la fin d'écriture*  
<sup>22</sup> *Alexis Fagot*



# Table of Contents

24	<b>Acknowledgements</b>	i
25	<b>Nederlandse samenvatting</b>	xvii
26	<b>English summary</b>	xix
27	<b>1 Introduction</b>	1-1
28	1.1 A story of High Energy Physics . . . . .	1-1
29	1.2 Organisation of this study . . . . .	1-1
30	<b>2 Investigating the TeV scale</b>	2-1
31	2.1 The Standard Model of Particle Physics . . . . .	2-1
32	2.2 The Large Hadron Collider and the Compact Muon Solenoid . . . . .	2-1
33	2.3 Muon Phase-II Upgrade . . . . .	2-1
34	<b>3 Amplification processes in gaseous detectors</b>	3-1
35	3.1 Signal formation . . . . .	3-1
36	3.2 Gas transport parameters . . . . .	3-1
37	<b>4 Resistive Plate Chambers</b>	4-1
38	4.1 Principle . . . . .	4-1
39	4.2 Rate capability of Resistive Plate Chambers . . . . .	4-1
40	4.3 High time resolution . . . . .	4-1
41	4.4 Resistive Plate Chambers at CMS . . . . .	4-1
42	4.4.1 Overview . . . . .	4-1
43	4.4.2 The present RPC system . . . . .	4-2
44	4.4.3 Pulse processing of CMS RPCs . . . . .	4-3
45	<b>5 Longevity studies and Consolidation of the present CMS RPC subsystem</b>	5-1
46	5.1 Testing detectors under extreme conditions . . . . .	5-1
47	5.1.1 The Gamma Irradiation Facilities . . . . .	5-3
48	5.1.1.1 GIF . . . . .	5-3
49	5.1.1.2 GIF++ . . . . .	5-5
50	5.2 Preliminary tests at GIF . . . . .	5-7
51	5.2.1 Resistive Plate Chamber test setup . . . . .	5-7
52	5.2.2 Data Acquisition . . . . .	5-9
53	5.2.3 Geometrical acceptance of the setup layout to cosmic muons . . . . .	5-9
54	5.2.3.1 Description of the simulation layout . . . . .	5-10
55	5.2.3.2 Simulation procedure . . . . .	5-12
56	5.2.3.3 Results . . . . .	5-13
57	5.2.4 Photon flux at GIF . . . . .	5-13

---

58	5.2.4.1	Expectations from simulations . . . . .	5-13
59	5.2.4.2	Dose measurements . . . . .	5-18
60	5.2.5	Results and discussions . . . . .	5-19
61	5.3	Longevity tests at GIF++ . . . . .	5-20
62	5.3.1	Description of the Data Acquisition . . . . .	5-23
63	5.3.2	RPC current, environmental and operation parameter monitoring . . . . .	5-24
64	5.3.3	Measurement procedure . . . . .	5-25
65	5.3.4	Longevity studies results . . . . .	5-25
66	<b>6</b>	<b>Investigation on high rate RPCs</b>	<b>6-1</b>
67	6.1	Rate limitations and ageing of RPCs . . . . .	6-1
68	6.1.1	Low resistivity electrodes . . . . .	6-1
69	6.1.2	Low noise front-end electronics . . . . .	6-1
70	6.2	Construction of prototypes . . . . .	6-1
71	6.3	Results and discussions . . . . .	6-1
72	<b>7</b>	<b>Conclusions and outlooks</b>	<b>7-1</b>
73	7.1	Conclusions . . . . .	7-1
74	7.2	Outlooks . . . . .	7-1
75	<b>A</b>	<b>A data acquisition software for CAEN VME TDCs</b>	<b>A-1</b>
76	A.1	GIF++ DAQ file tree . . . . .	A-1
77	A.2	Usage of the DAQ . . . . .	A-2
78	A.3	Description of the readout setup . . . . .	A-3
79	A.4	Data read-out . . . . .	A-3
80	A.4.1	V1190A TDCs . . . . .	A-4
81	A.4.2	DataReader . . . . .	A-6
82	A.4.3	Data quality flag . . . . .	A-10
83	A.5	Communications . . . . .	A-12
84	A.5.1	V1718 USB Bridge . . . . .	A-13
85	A.5.2	Configuration file . . . . .	A-13
86	A.5.3	WebDCS/DAQ intercommunication . . . . .	A-17
87	A.5.4	Example of inter-process communication cycle . . . . .	A-18
88	A.6	Software export . . . . .	A-18
89	<b>B</b>	<b>Details on the offline analysis package</b>	<b>B-1</b>
90	B.1	GIF++ Offline Analysis file tree . . . . .	B-1
91	B.2	Usage of the Offline Analysis . . . . .	B-2
92	B.2.1	Output of the offline tool . . . . .	B-3
93	B.2.1.1	ROOT file . . . . .	B-3
94	B.2.1.2	CSV files . . . . .	B-5
95	B.3	Analysis inputs and information handling . . . . .	B-6
96	B.3.1	Dimensions file and IniFile parser . . . . .	B-6
97	B.3.2	TDC to RPC link file and Mapping . . . . .	B-7
98	B.4	Description of GIF++ setup within the Offline Analysis tool . . . . .	B-8
99	B.4.1	RPC objects . . . . .	B-9
100	B.4.2	Trolley objects . . . . .	B-9
101	B.4.3	Infrastructure object . . . . .	B-10
102	B.5	Handeling of data . . . . .	B-12
103	B.5.1	RPC hits . . . . .	B-12

---

104	B.5.2 Clusters of hits . . . . .	B-13
105	<b>C Structure of the hybrid simulation software</b>	<b>C-1</b>
106	C.1 Introduction . . . . .	C-1



# List of Figures

107

108      2.1	Absorbed dose in the CMS cavern after an integrated luminosity of 3000 fb. R is the transverse distance from the beamline and Z is the distance along the beamline from the Interaction Point at Z=0. . . . .	2-2
109      2.2	A quadrant of the muon system, showing DTs (yellow), RPCs (light blue), and CSCs (green). The locations of new forward muon detectors for Phase-II are contained within the dashed box and indicated in red for GEM stations (ME0, GE1/1, and GE2/1) and dark blue for improved RPC (iRPC) stations (RE3/1 and RE4/1). . . . .	2-2
110      2.3	RMS of the multiple scattering displacement as a function of muon $p_T$ for the proposed forward muon stations. All of the electromagnetic processes such as bremsstrahlung and magnetic field effect are included in the simulation. . . . .	2-3
111      4.1	Signals from the RPC strips are shaped by the FEE described on Figure 4.1a. Output LVDS signals are then read-out by a TDC module connected to a computer or converted into NIM and sent to scalers. Figure 4.1b describes how these converted signals are put in coincidence with the trigger. . . . .	4-3
112      4.2	Description of the principle of a CFD. A comparison of threshold triggering (left) and constant fraction triggering (right) is shown in Figure 4.2a. Constant fraction triggering is obtained thanks to zero-crossing technique as explained in Figure 4.2b. The signal arriving at the input of the CFD is split into three components. A first one is delayed and connected to the inverting input of a first comparator. A second component is connected to the noninverting input of this first comparator. A third component is connected to the noninverting input of another comparator along with a threshold value connected to the inverting input. Finally, the output of both comparators is fed through an AND gate. . . . .	4-4
113      5.1	(5.1a) Extrapolation from 2016 data of single hit rate per unit area in the barrel region. (5.1b) Extrapolation from 2016 data of single hit rate per unit area in the endcap region. . . . .	5-2
114      5.2	Background Fluka simulation compared to 2016 Data at $L = 10^{34} \text{ cm}^{-2} \cdot \text{s}^{-1}$ in the fourth endcap disk region. A mismatch in between simulation and data can be observed. [To be understood.] . . . . .	5-3
115      5.3	Layout of the test beam zone called X5c GIF at CERN. Photons from the radioactive source produce a sustained high rate of random hits over the whole area. The zone is surrounded by 8 m high and 80 cm thick concrete walls. Access is possible through three entry points. Two access doors for personnel and one large gate for material. A crane allows installation of heavy equipment in the area. . . . .	5-4
116      5.4	$^{137}\text{Cs}$ decays by $\beta^-$ emission to the ground state of $^{137}\text{Ba}$ (BR = 5.64%) and via the 662 keV isomeric level of $^{137}\text{Ba}$ (BR = 94.36%) whose half-life is 2.55 min. . . . .	5-5

144	5.5	Floor plan of the GIF++ facility. When the facility downstream of the GIF++ takes electron beam, a beam pipe is installed along the beam line (z-axis). The irradiator can be displaced laterally (its center moves from $x = 0.65$ m to 2.15 m), to increase the distance to the beam pipe. . . . .	5-5
145	5.6	Simulated unattenuated current of photons in the xz plane (Figure 5.6a) and yz plane (Figure 5.6b) through the source at $x = 0.65$ m and $y = 0$ m. With angular correction filters, the current of 662 keV photons is made uniform in xy planes. . . . .	5-6
146	5.7	Description of the RPC setup. Dimensions are given in mm. A tent containing RPCs is placed at 1720 mm from the source container. The source is situated in the center of the container. RE-4-2-BARC-161 chamber is 160 mm inside the tent. This way, the distance between the source and the chambers plan is 2060 mm. Figure 5.7a provides a side view of the setup in the xz plane while Figure 5.7b shows a top view in the yz plane. . . . .	5-7
147	5.8	RE-4-2-BARC-161 chamber is inside the tent as described in Figure 5.7. In the top right, the two scintillators used as trigger can be seen. This trigger system has an inclination of 10° relative to horizontal and is placed above half-partition B2 of the RPCs. PMT electronics are shielded thanks to lead blocks placed in order to protect them without stopping photons from going through the scintillators and the chamber. . . . .	5-8
148	5.9	Hit distributions over all 3 partitions of RE-4-2-BARC-161 chamber is showed on these plots. Top, middle and bottom figures respectively correspond to partitions A, B, and C. These plots show that some events still occur in other half-partitions than B2, which corresponds to strips 49 to 64, in front of which the trigger is placed, contributing to the inefficiency of detection of cosmic muons. In the case of partitions A and C, the very low amount of data can be interpreted as noise. On the other hand, it is clear that a little portion of muons reach the half-partition B1, corresponding to strips 33 to 48. . . . .	5-9
149	5.10	Results are derived from data taken on half-partition B2 only. On the 18 <sup>th</sup> of June 2014, data has been taken on chamber RE-2-BARC-161 at building 904 (Prevessin Site) with cosmic muons providing us a reference efficiency plateau of $(97.54 \pm 0.15)\%$ represented by a black curve. A similar measurement has been done at GIF on the 21 <sup>st</sup> of July with the same chamber giving a plateau of $(78.52 \pm 0.94)\%$ represented by a red curve. . . . .	5-10
150	5.11	Representation of the layout used for the simulations of the test setup. The RPC is represented as a yellow trapezoid while the two scintillators as blue cuboids looking at the sky. A green plane corresponds to the muon generation plane within the simulation. Figure 5.7a shows a global view of the simulated setup. Figure 5.7b shows a zommed view that allows to see the 2 scintillators as well as the full RPC plane. . . . .	5-11
151	5.12	$\gamma$ flux $F(D)$ is plot using values from table 5.1. As expected, the plot shows similar attenuation behaviours with increasing distance for each absorption factors. . . . .	5-14
152	5.13	Figure 5.13a shows the linear approximation fit done via formulae 5.7 on data from table 5.2. Figure 5.13b shows a comparison of this model with the simulated flux using a and b given in figure 5.13a in formulae 5.4 and the reference value $D_0 = 50\text{cm}$ and the associated flux for each absorption factor $F_0^{ABS}$ from table 5.1 . . . . .	5-16
153	5.14	Dose measurements has been done in a plane corresponding to the tents front side. This plan is 1900 mm away from the source. As explained in the first chapter, a lens-shaped lead filter provides a uniform photon flux in the vertical plan orthogonal to the beam direction. If the second line of measured fluxes is not taken into account because of lower values due to experimental equipments in the way between the source and the tent, the uniformity of the flux is well showed by the results. . . . .	5-18
154			
155			
156			
157			
158			
159			
160			
161			
162			
163			
164			
165			
166			
167			
168			
169			
170			
171			
172			
173			
174			
175			
176			
177			
178			
179			
180			
181			
182			
183			
184			
185			
186			
187			
188			
189			
190			
191			
192			

---

193	5.15 . . . . .	5-19
194	5.16 Evolution of the maximum efficiency for RE2 (5.16a) and RE4 (5.16b) chambers	
195	with increasing extrapolated $\gamma$ rate per unit area at working point. Both irradiated	
196	(blue) and non irradiated (red) chambers are shown. . . . .	5-21
197	5.17 Evolution of the working point for RE2 (5.17a) and RE4 (5.17b) with increasing	
198	extrapolated $\gamma$ rate per unit area at working point. Both irradiated (blue) and non	
199	irradiated (red) chambers are shown. . . . .	5-21
200	5.18 Evolution of the maximum efficiency at HL-LHC conditions, i.e. a background hit	
201	rate per unit area of 300 Hz/cm <sup>2</sup> , with increasing integrated charge for RE2 (5.18a)	
202	and RE4 (5.18b) detectors. Both irradiated (blue) and non irradiated (red) chambers	
203	are shown. The integrated charge for non irradiated detectors is recorded during test	
204	beam periods and stays small with respect to the charge accumulated in irradiated	
205	chambers. . . . .	5-22
206	5.19 Comparison of the efficiency sigmoid before (triangles) and after (circles) irradiation	
207	for RE2 (5.19a) and RE4 (5.19b) detectors. Both irradiated (blue) and non irradiated	
208	(red) chambers are shown. . . . .	5-22
209	5.20 Evolution of the Bakelite resistivity for RE2 (5.20a) and RE4 (5.20b) detectors. Both	
210	irradiated (blue) and non irradiated (red) chambers are shown. . . . .	5-23
211	5.21 Evolution of the noise rate per unit area for the irradiated chamber RE2-2-BARC-9	
212	only. . . . .	5-23
213	A.1 (A.1a) View of the front panel of a V1190A TDC module [10]. (A.1b) View of the	
214	front panel of a V1718 Bridge module [11]. (A.1c) View of the front panel of a 6U	
215	6021 VME crate [12]. . . . .	A-3
216	A.2 Module V1190A <i>Trigger Matching Mode</i> timing diagram [10]. . . . .	A-4
217	A.3 Structure of the ROOT output file generated by the DAQ. The 5 branches ( <code>EventNumber</code> ,	
218	<code>number_of_hits</code> , <code>Quality_flag</code> , <code>TDC_channel</code> and <code>TDC_TimeStamp</code> ) are visible on	
219	the left panel of the ROOT browser. On the right panel is visible the histogram cor-	
220	responding to the variable <code>nHits</code> . In this specific example, there were approximately	
221	50k events recorded to measure the gamma irradiation rate on the detectors. Each	
222	event is stored as a single entry in the <code>TTree</code> . . . . .	A-10
223	A.4 The effect of the quality flag is explained by presenting the content of <code>TBranch</code>	
224	<code>number_of_hits</code> of a data file without <code>Quality_flag</code> in Figure A.4a and the con-	
225	tent of the same <code>TBranch</code> for data corresponding to a <code>Quality_flag</code> where all TDCs	
226	were labelled as <code>GOOD</code> in Figure A.4b taken with similar conditions. It can be noted	
227	that the number of entries in Figure A.4b is slightly lower then in Figure A.4a due	
228	to the excluded events. . . . .	A-12
229	A.5 Using the same data as previously showed in Figure A.4, the effect of the quality	
230	flag is explained by presenting the reconstructed hit multiplicity of a data file with-	
231	out <code>Quality_flag</code> in Figure A.5a and the reconstructed content of the same RPC	
232	partition for data corresponding to a <code>Quality_flag</code> where all TDCs were labelled as	
233	<code>GOOD</code> in Figure A.5b taken with similar conditions. The artificial high content of bin	
234	0 is completely suppressed. . . . .	A-12
235	A.6 WebDCS DAQ scan page. On this page, shifters need to choose the type of scan	
236	(Rate, Efficiency or Noise Reference scan), the gamma source configuration at the	
237	moment of data taking, the beam configuration, and the trigger mode. These in-	
238	formation will be stored in the DAQ ROOT output. Are also given the minimal	
239	measurement time and waiting time after ramping up of the detectors is over before	
240	starting the data acquisition. Then, the list of HV points to scan and the number of	
241	triggers for each run of the scan are given in the table underneath. . . . .	A-14



## List of Tables

242

243	5.1	Total photon flux ( $E\gamma \leq 662$ keV) with statistical error predicted considering a $^{137}\text{Cs}$ activity of 740 GBq at different values of the distance $D$ to the source along the x-axis of irradiation field [6]. . . . .	5-13
244	5.2	Correction factor $c$ is computed thanks to formulae 5.5 taking as reference $D_0 =$ 50 cm and the associated flux $F_0^{ABS}$ for each absorption factor available in table 5.1. . . . .	5-15
245	5.3	The data at $D_0$ in 1997 is taken from [6]. In a second step, using Equations 5.8 and 5.9, the flux at $D$ can be estimated in 1997. Then, taking into account the attenuation of the source activity, the flux at $D$ can be estimated at the time of the tests in GIF in 2014. Finally, assuming a sensitivity of the RPC to $\gamma$ $s = 2 \cdot 10^{-3}$ , an estimation of the hit rate per unit area is obtained. . . . .	5-17
246	A.1	Inter-process communication cycles in between the webDCS and the DAQ through file string signals. . . . .	A-19
247			
248			
249			
250			
251			
252			
253			
254			



255

## List of Acronyms

256

### List of Acronyms

257

258

#### A

259

260

261

AFL

Almost Full Level

262

263

#### B

264

265

266 BARC

Bhabha Atomic Research Centre

267 BLT

Block Transfer

268 BR

Branching Ratio

269

270

#### C

271

272

273 CAEN

Costruzioni Apparecchiature Elettroniche Nucleari S.p.A.

274 CERN

European Organization for Nuclear Research

275 CFD

Constant Fraction Discriminator

276 CMS

Compact Muon Solenoid

277 CSC

Cathode Strip Chamber

278

279

#### D

280

281

282 DAQ

Data Acquisition

283 DCS

Detector Control Software

284 DQM

Data Quality Monitoring

285 DT

Drift Tube

286

287

#### F

288

289

290	FEE	Front-End Electronics
291	FEB	Front-End Board
292		
293	<b>G</b>	
294		
295		
296	GE-/-	Find a good description
297	GE1/1	Find a good description
298	GE2/1	Find a good description
299	GEANT	GEometry ANd Tracking - a series of software toolkit platforms developed by CERN
300		
301	GEM	Gas Electron Multiplier
302	GIF	Gamma Irradiation Facility
303	GIF++	new Gamma Irradiation Facility
304		
305	<b>H</b>	
306		
307		
308	HL-LHC	High Luminosity LHC
309	HV	High Voltage
310		
311	<b>I</b>	
312		
313		
314	iRPC	improved RPC
315	IRQ	Interrupt Request
316		
317	<b>L</b>	
318		
319		
320	LHC	Large Hadron Collider
321	LS1	First Long Shutdown
322	LS3	Third Long Shutdown
323	LV	Low Voltage
324	LVDS	Low-Voltage Differential Signaling
325		
326	<b>M</b>	
327		
328		
329	MC	Monte Carlo
330	MCNP	Monte Carlo N-Particle
331	ME-/-	Find good description
332	ME0	Find good description

---

333		
334	<b>N</b>	
335		
336		
337	<b>NIM</b>	Nuclear Instrumentation Module logic signals
338		
339	<b>P</b>	
340		
341		
342	<b>PMT</b>	PhotoMultiplier Tube
343		
344	<b>R</b>	
345		
346		
347	<b>RE-/-</b>	Find a good description
348	<b>RE2/2</b>	Find a good description
349	<b>RE3/1</b>	Find a good description
350	<b>RE3/2</b>	Find a good description
351	<b>RE4/1</b>	Find a good description
352	<b>RE4/2</b>	Find a good description
353	<b>RE4/3</b>	Find a good description
354	<b>RMS</b>	Root Mean Square
355	<b>ROOT</b>	a framework for data processing born at CERN
356	<b>RPC</b>	Resistive Plate Chamber
357		
358	<b>S</b>	
359		
360		
361	<b>SPS</b>	Super Proton Synchrotron
362		
363	<b>T</b>	
364		
365		
366	<b>TDC</b>	Time-to-Digital Converter
367		
368	<b>W</b>	
369		
370		
371	<b>webDCS</b>	Web Detector Control System



<sup>373</sup>

## Nederlandse samenvatting –Summary in Dutch–

<sup>374</sup>

<sup>375</sup> Le resume en Neerlandais (j'aurais peut-être de apprendre la langue juste pour ca...).



## English summary

<sup>377</sup> Le meme résume mais en Anglais (on commencera par la hein!).



# 1

## Introduction

378

379

<sup>380</sup> **1.1 A story of High Energy Physics**

<sup>381</sup> **1.2 Organisation of this study**



# 2

382

383

## Investigating the TeV scale

384

### 2.1 The Standard Model of Particle Physics

385

### 2.2 The Large Hadron Collider and the Compact Muon Solenoid

386

### 2.3 Muon Phase-II Upgrade

387

After the more than two years lasting First Long Shutdown (LS1), the Large Hadron Collider (LHC) delivered its very first Run-II proton-proton collisions early 2015. LS1 gave the opportunity to the LHC and to its experiments to undergo upgrades. The accelerator is now providing collisions at center-of-mass energy of 13 TeV and bunch crossing rate of 40 MHz, with a peak luminosity exceeding its design value. During the first and upcoming second LHC Long Shutdown, the Compact Muon Solenoid (CMS) detector is also undergoing a number of upgrades to maintain a high system performance [1].

394

From the LHC Phase-II or High Luminosity LHC (HL-LHC) period onwards, i.e. past the Third Long Shutdown (LS3), the performance degradation due to integrated radiation as well as the average number of inelastic collisions per bunch crossing, or pileup, will rise substantially and become a major challenge for the LHC experiments, like CMS that are forced to address an upgrade program for Phase-II [2]. Simulations of the expected distribution of absorbed dose in the CMS detector under HL-LHC conditions, show in figure 5.14 that detectors placed close to the beamline will have to withstand high irradiation, the radiation dose being of the order of a few tens of Gy.

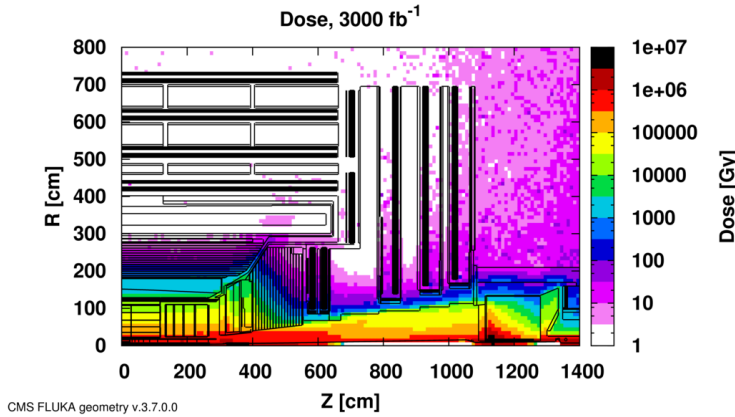


*Figure 2.1: Absorbed dose in the CMS cavern after an integrated luminosity of 3000 fb<sup>-1</sup>. R is the transverse distance from the beamline and Z is the distance along the beamline from the Interaction Point at Z=0.*

The measurement of small production cross-section and/or decay branching ratio processes, such as the Higgs boson coupling to charge leptons or the  $B_s \rightarrow \mu^+\mu^-$  decay, is of major interest and specific upgrades in the forward regions of the detector will be required to maximize the physics acceptance on the largest possible solid angle. To ensure proper trigger performance within the present coverage, the muon system will be completed with new chambers. In figure 2.2 one can see that the existing Cathode Strip Chambers (CSCs) will be completed by Gas Electron Multipliers (GEMs) and Resistive Plate Chambers (RPCs) in the pseudo-rapidity region  $1.6 < |\eta| < 2.4$  to complete its redundancy as originally scheduled in the CMS Technical Proposal [3].

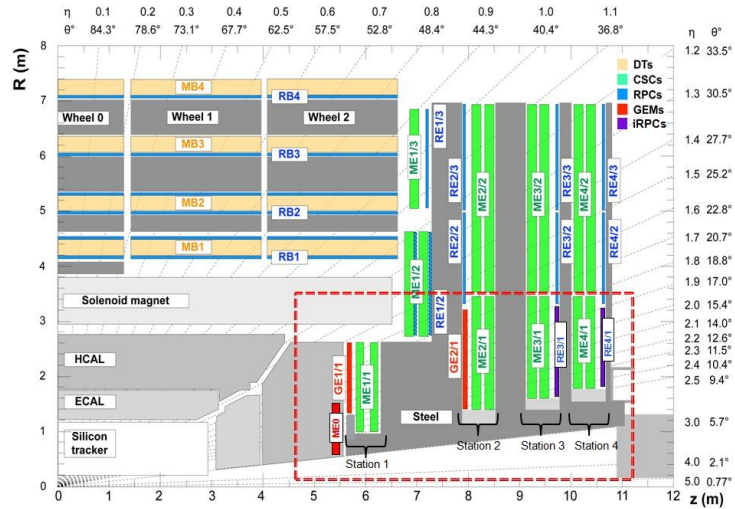


*Figure 2.2: A quadrant of the muon system, showing DTs (yellow), RPCs (light blue), and CSCs (green). The locations of new forward muon detectors for Phase-II are contained within the dashed box and indicated in red for GEM stations (ME0, GE1/1, and GE2/1) and dark blue for improved RPC (iRPC) stations (RE3/1 and RE4/1).*

RPCs are used by the CMS first level trigger for their good timing performances. Indeed, a very

410 good bunch crossing identification can be obtained with the present CMS RPC system, given their  
 411 fast response of the order of 1 ns. In order to contribute to the precision of muon momentum mea-  
 412 surements, muon chambers should have a spatial resolution less or comparable to the contribution  
 413 of multiple scattering [1]. Most of the plausible physics is covered only considering muons with  
 414  $p_T < 100$  GeV thus, in order to match CMS requirements, a spatial resolution of  $\mathcal{O}(\text{few mm})$  the  
 415 proposed new RPC stations, as shown by the simulation in figure 2.3. According to preliminary  
 416 designs, RE3/1 and RE4/1 readout pitch will be comprised between 3 and 6 mm and 5  $\eta$ -partitions  
 417 could be considered.

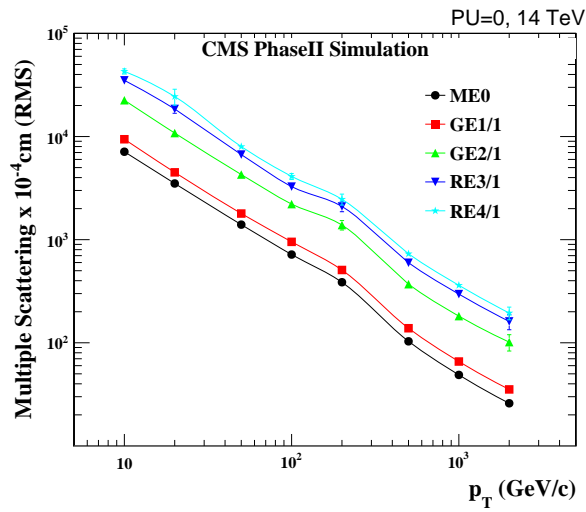


Figure 2.3: RMS of the multiple scattering displacement as a function of muon  $p_T$  for the proposed forward muon stations. All of the electromagnetic processes such as bremsstrahlung and magnetic field effect are included in the simulation.



# 3

418

419

## Amplification processes in gaseous detectors

420 **3.1 Signal formation**

421 **3.2 Gas transport parameters**



# 4

422

423

## Resistive Plate Chambers

424 **4.1 Principle**

425 **4.2 Rate capability of Resistive Plate Chambers**

426 **4.3 High time resolution**

427 **4.4 Resistive Plate Chambers at CMS**

428 **4.4.1 Overview**

429 The Resistive Plate Chambers (RPC) system, located in both barrel and endcap regions, provides a  
430 fast, independent muon trigger with a looser  $p_T$  threshold over a large portion of the pseudorapidity  
431 range ( $|\eta| < 1.6$ ) [add reconstruction].

432

433 During High-Luminosity LHC (HL-LHC) operations the expected conditions in terms of back-  
434 ground and pile-up will make the identification and correct  $P_T$  assignment a challenge for the Muon  
435 system. The goal of RPC upgrade is to provide additional hits to the Muon system with precise tim-  
436 ing. All these informations will be elaborated by the trigger system in a global way enhancing the  
437 performance of the trigger in terms of efficiency and rate control. The RPC Upgrade is based on two  
438 projects: an improved Link Board System and the extension of the RPC coverage up to  $|\eta| = 2.4$ .  
439 [FIXME 2.4 or 2.5?]

440 The Link Board system, that will be described in section xxx, is responsible to process, syn-  
441 chronize and zero-suppress the signals coming from the RPC front end boards. The Link Board  
442 components have been produced between 2006 and 2007 and will be subjected to aging and failure  
443 in the long term. The upgraded Link Board system will overcome the aging problems described in  
444 section xxx and will allow for a more precise timing information to the RPC hits from 25 to 1 ns [ref  
445 section xxx].

446 The extension of the RPC system up to  $|\eta| = 2.1$  was already planned in the CMS TDR [ref  
 447 cmstdr] and staged because of budget limitations and expected background rates higher than the rate  
 448 capability of the present CMS RPCs in that region. An extensive R&D program has been done in  
 449 order to develop an improved RPC that fulfills the CMS requirements. Two new RPC layers in the  
 450 innermost ring of stations 3 and 4 will be added with benefits to the neutron-induced background  
 451 reduction and efficiency improvement for both trigger and offline reconstruction.

#### 452 4.4.2 The present RPC system

453 The RPC system is organized in 4 stations called RB1 to RB4 in the barrel region, and RE1 to RE4  
 454 in the endcap region. The innermost barrel stations, RB1 and RB2, are instrumented with 2 layers  
 455 of RPCs facing the innermost (RB1in and RB2in) and outermost (RB1out and RB2out) sides of the  
 456 DT chambers. Every chamber is then divided from the read-out point of view into 2 or 3  $\eta$  partitions  
 457 called “rolls”. The RPC system consist of 480 barrel chambers and 576 endcap chambers. Details  
 458 on the geometry are discussed in the paper [ref to geo paper].

459 The CMS RPC chamber is a double-gap, operated in avalanche mode to ensure reliable operation  
 460 at high rates. Each RPC gap consists of two 2-mm-thick resistive High-Pressure Laminate (HPL)  
 461 plates separated by a 2-mm-thick gas gap. The outer surface of the HPL plates is coated with a thin  
 462 conductive graphite layer, and a voltage is applied. The RPCs are operated with a 3-component,  
 463 non-flammable gas mixture consisting of 95.2% freon ( $C_2H_2F_4$ , known as R134a), 4.5% isobutane  
 464 ( $i-C_4H_{10}$ ), and 0.3% sulphur hexafluoride ( $SF_6$ ) with a relative humidity of 40% - 50%. Readout  
 465 strips are aligned in  $\eta$  between the 2 gas gaps. [\[Add a sentence on FEBs.\]](#)

466 The discriminated signals coming from the Front End boards feed via twisted cables (10 to 20 m  
 467 long) the Link Board System located in UXC on the balconies around the detector. The Link System  
 468 consist of the 1376 Link Boards (LBs) and the 216 Control Boards (CBs), placed in 108 Link Boxes.  
 469 The Link Box is a custom crate (6U high) with 20 slots (for two CBs and eighteen LBs). The Link  
 470 Box contains custom backplane to which the cables from the chambers are connected, as well as the  
 471 cables providing the LBs and CBs power supply and the cables for the RPC FEBs control with use  
 472 of the I2C protocol (trough the CB). The backplane itself contains only connectors (and no any other  
 473 electronic devices).

474 The Link Board has 96 input channels (one channel corresponds to one RPC strip). The input  
 475 signals are the  $\sim 100$  ns binary pulses which are synchronous to the RPC hits, but not to the LHC  
 476 clock (which drives the entire CMS electronics). Thus the first step of the FEB signals processing  
 477 is synchronization, i.e. assignment of the signals to the BXes (25 ns periods). Then the data are  
 478 compressed with a simple zero-suppressing algorithm (the input channels are grouped into 8 bit  
 479 partitions, only the partitions with at least one nonzero bit are selected for each BX). Next, the non-  
 480 empty partitions are time-multiplexed i.e. if there are more than one such partition in a given BX,  
 481 they are sent one-by-one in consecutive BXes. The data from 3 neighbouring LBs are concentrated  
 482 by the middle LB which contains the optical transmitter for sending them to the USC over a fiber at  
 483 1.6 Gbps.

484 The Control Boards provide the communication of the control software with the LBs via the  
 485 FEC/CCU system. The CBs are connected into token rings, each ring consists of 12 CBs of one  
 486 detector tower and a FEC mezzanine board placed on the CCS board located in the VME crate in  
 487 the USC. In total, there are 18 rings in the entire Link System. The CBs also perform automatic  
 488 reloading of the LB's firmware which is needed in order to avoid accumulation of the radiation  
 489 induced SEUs in the LBs firmware.

490 Both LBs and CB are based on the Xilinx Spartan III FPGAs, the CB additionally contains  
 491 radiation-tolerant (FLASH based) FPGA Actel ProAsicPlus.

492 The High Voltage power system is located in USC, not exposed to radiation and easily accessible  
 493 for any reparation. A single HV channel powers 2 RPC chambers both in the barrel and endcap  
 494 regions. The Low Voltage boards are located in UXC on the balconies and provide the voltage to the  
 495 front end electronics.

#### 496 4.4.3 Pulse processing of CMS RPCs

497 Signals induced by cosmic particle in the RPC strips are shaped by standard CMS RPC Front-End  
 498 Electronics (FEE) following the scheme of Figure 4.1. On a first stage, analogic signals are amplified  
 499 and then sent to the Constant Fraction Discriminator (CFD) described in Figure 4.2. At the end of  
 500 the chain, 100 ns long pulses are sent in the LVDS output. These output signal are sent on one side to  
 501 a V1190A Time-to-Digital Converter (TDC) module from CAEN and on the other to an OR module  
 502 to count the number of detected signals. Trigger and hit coïncidences are monitored using scalers.  
 503 The TDC is used to store the data into ROOT files. These files are thus analysed to understand the  
 504 detectors performance.

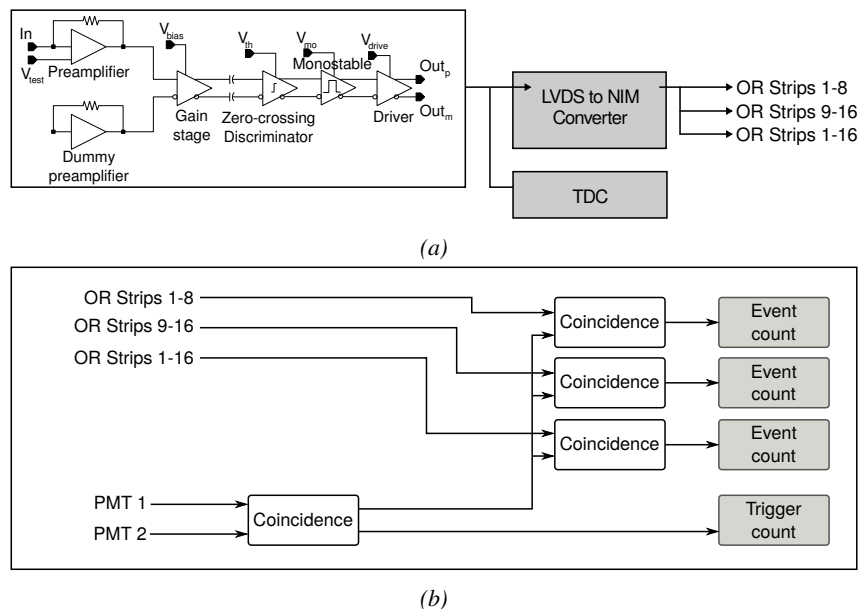
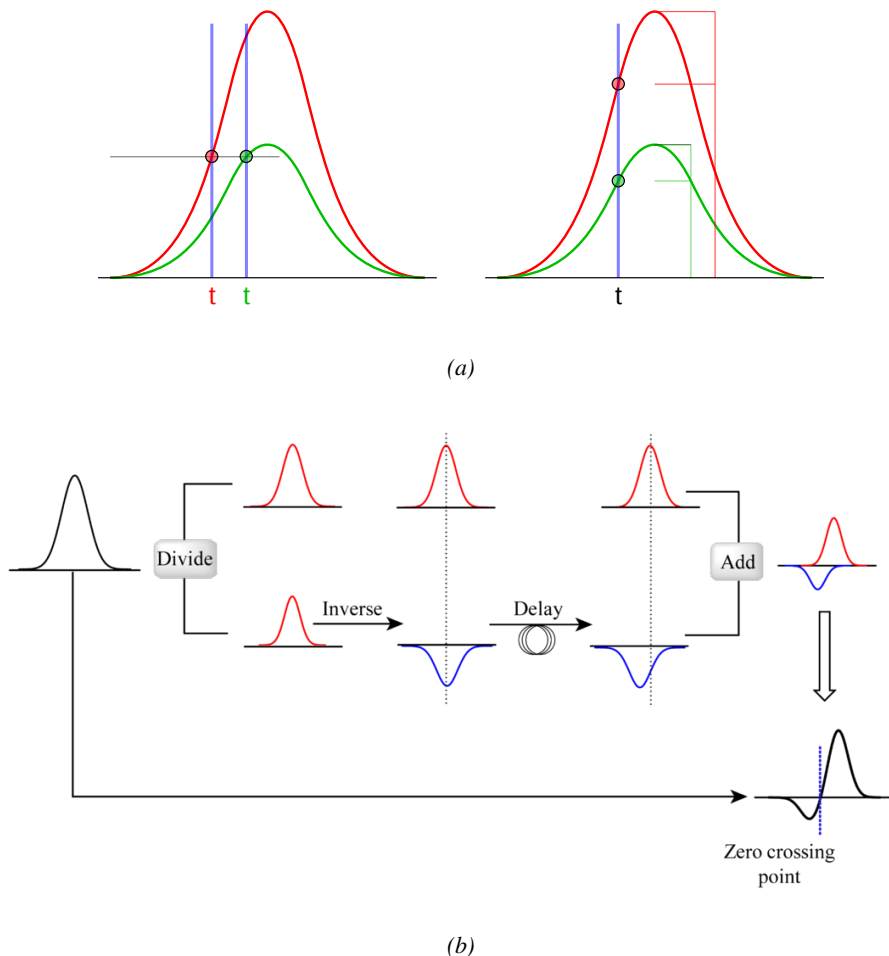


Figure 4.1: Signals from the RPC strips are shaped by the FEE described on Figure 4.1a. Output LVDS signals are then read-out by a TDC module connected to a computer or converted into NIM and sent to scalers. Figure 4.1b describes how these converted signals are put in coincidence with the trigger.



*Figure 4.2: Description of the principle of a CFD. A comparison of threshold triggering (left) and constant fraction triggering (right) is shown in Figure 4.2a. Constant fraction triggering is obtained thanks to zero-crossing technique as explained in Figure 4.2b. The signal arriving at the input of the CFD is split into three components. A first one is delayed and connected to the inverting input of a first comparator. A second component is connected to the noninverting input of this first comparator. A third component is connected to the noninverting input of another comparator along with a threshold value connected to the inverting input. Finally, the output of both comparators is fed through an AND gate.*

# 5

505

506

507

## Longevity studies and Consolidation of the present CMS RPC subsystem

508

### 5.1 Testing detectors under extreme conditions

509

The upgrade from LHC to HL-LHC will increase the peak luminosity from  $10^{34} \text{ cm}^{-2} \text{ s}^{-1}$  to reach  $5 \times 10^{34} \text{ cm}^{-2} \text{ s}^{-1}$ , increasing in the same way the total expected background to which the RPC system will be subjected to. Composed of low energy gammas and neutrons from  $p\text{-}p$  collisions, low momentum primary and secondary muons, puch-through hadrons from calorimeters, and particles produced in the interaction of the beams with collimators, the background will mostly affect the regions of CMS that are the closest to the beam line, i.e. the RPC detectors located in the endcaps.

[To update.]

510

511

512

513

514

515

516

517

The 2016 data allowed to study the values of the background rate in all RPC system. In Figure 5.1, the distribution of the chamber background hit rate per unit area is shown at a luminosity of  $5 \times 10^{34} \text{ cm}^{-2} \cdot \text{s}^{-1}$  linearly extrapolating from data collected in 2016 [ref mentioning the linear dependency of rate vs lumi]. The maximum rate per unit area at HL-LHC conditions is expected to be of the order of  $600 \text{ Hz/cm}^2$  (including a safety factor 3). Nevertheless, Fluka simulations have conducted in order to understand the background at HL-LHC conditions. The comparison to the data has shown, in Figure 5.2, a discrepancy of a factor 2 even though the order of magnitude is consistent. [Understand mismatch.]

518

519

520

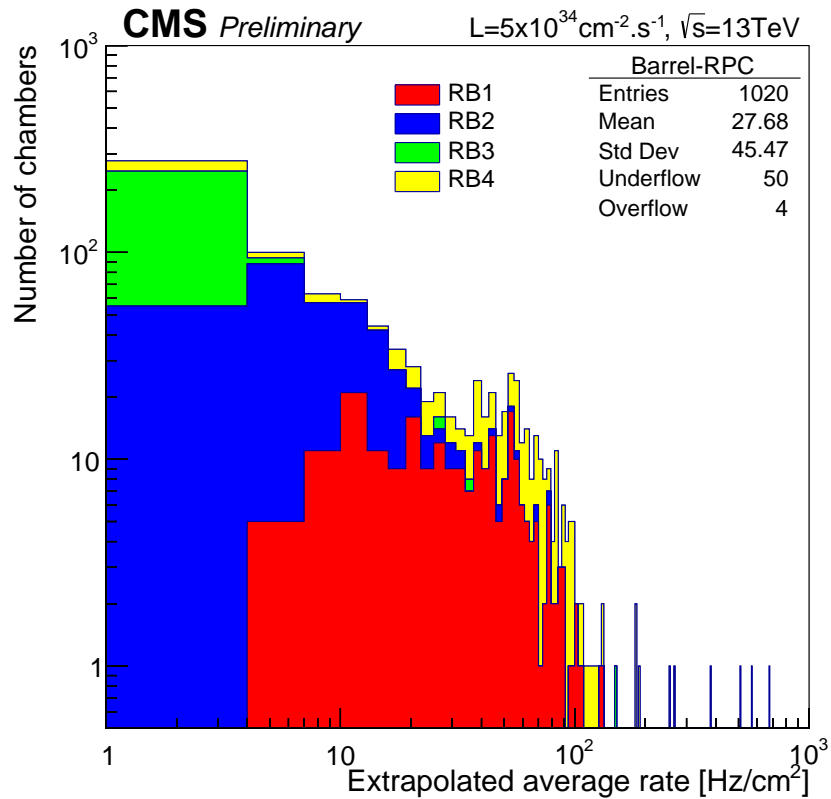
521

522

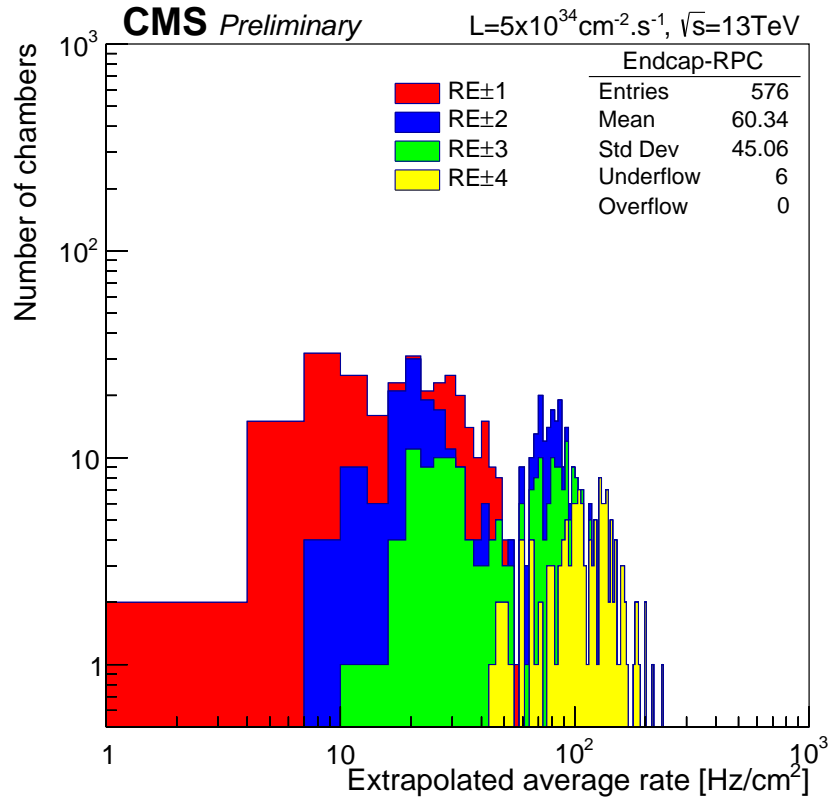
523

524

525



(a)



(b)

Figure 5.1: (5.1a) Extrapolation from 2016 data of single hit rate per unit area in the barrel region. (5.1b) Extrapolation from 2016 data of single hit rate per unit area in the endcap region.

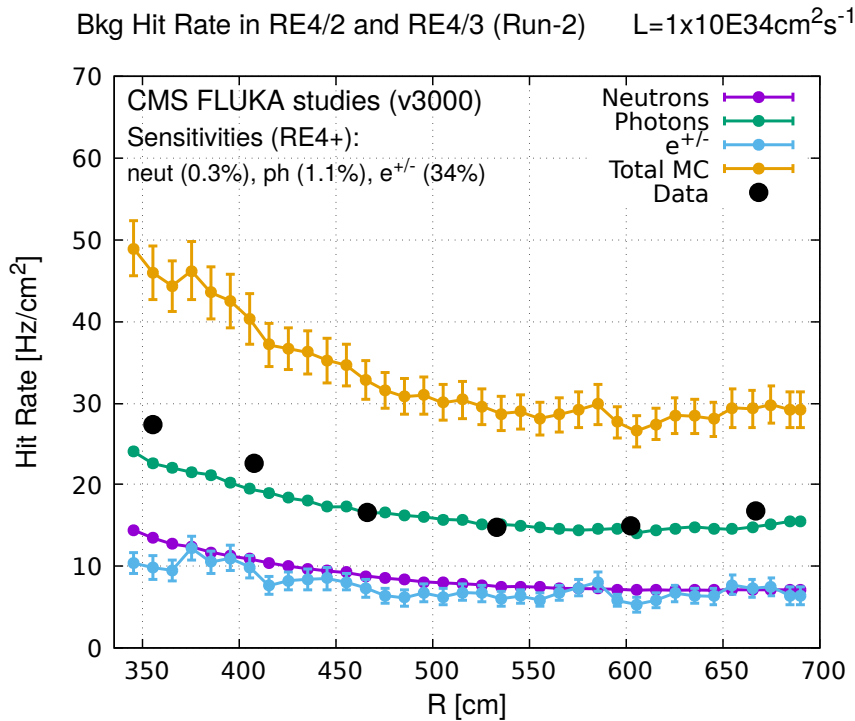


Figure 5.2: Background Fluka simulation compared to 2016 Data at  $L = 10^{34}\text{cm}^{-2}\text{s}^{-1}$  in the fourth endcap disk region. A mismatch in between simulation and data can be observed. [\[To be understood.\]](#)

526 In the past, extensive long-term tests were carried out at several gamma and neutron facilities  
 527 certifying the detector performance. Both full size and small prototype RPCs have been irradiated  
 528 with photons up to an integrated charge of  $\sim 0.05\text{C}/\text{cm}^2$  and  $\sim 0.4\text{C}/\text{cm}^2$ , respectively [4, 5].  
 529 During Run-I, the RPC system provided stable operation and excellent performance and did not  
 530 show any aging effects for integrated charge of the order of  $0.01\text{C}/\text{cm}^2$ . Projections on currents  
 531 from 2016 Data, has allowed to determine that the total integrated charge, by the end of HL-LHC,  
 532 would be of the order of  $1\text{C}/\text{cm}^2$  (including a safety factor 3). [\[Corresponding figure needed.\]](#)

533

### 534 5.1.1 The Gamma Irradiation Facilities

#### 535 5.1.1.1 GIF

536 Located in the SPS West Area at the downstream end of the X5 test beam, the Gamma Irradiation  
 537 Facility (GIF) was a test area in which particle detectors were exposed to a particle beam in presence  
 538 of an adjustable gamma background [6]. Its goal was to reproduce background conditions these  
 539 detectors would suffer in their operating environment at LHC. GIF layout is shown in Figure 5.3.  
 540 Gamma photons are produced by a strong  $^{137}\text{Cs}$  source installed in the upstream part of the zone  
 541 inside a lead container. The source container includes a collimator, designed to irradiate a  $6 \times 6\text{ m}^2$   
 542 area at 5 m maximum to the source. A thin lens-shaped lead filter helps providing with a uniform  
 543 outcoming flux in a vertical plane, orthogonal to the beam direction. The principal collimator hole  
 544 provides a pyramidal aperture of  $74^\circ \times 74^\circ$  solid angle and provides a photon flux in a pyramidal vol-

ume along the beam axis. The photon rate is controled by further lead filters allowing the maximum rate to be limited and to vary within a range of four orders of magnitude. Particle detectors under test are then placed within the pyramidal volume in front of the source, perpendicularly to the beam line in order to profit from the homogeneous photon flux. Adjusting the background flux of photons can then be done by using the filters and choosing the position of the detectors with respect to the source.

550

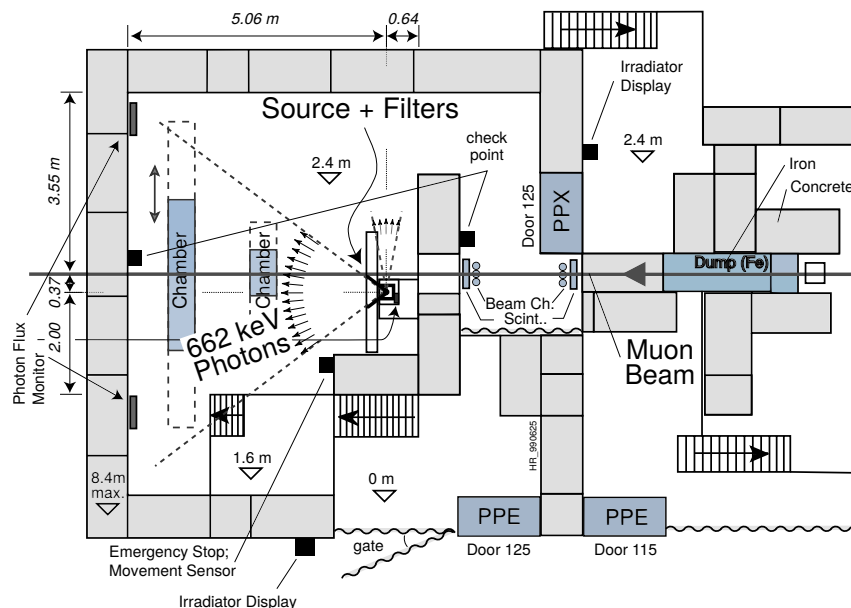


*Figure 5.3: Layout of the test beam zone called X5c GIF at CERN. Photons from the radioactive source produce a sustained high rate of random hits over the whole area. The zone is surrounded by 8 m high and 80 cm thick concrete walls. Access is possible through three entry points. Two access doors for personnel and one large gate for material. A crane allows installation of heavy equipment in the area.*

As described on Figure 5.4, the  $^{137}\text{Cs}$  source emits a 662 keV photon in 85% of the decays. An activity of 740 GBq was measured on the 5<sup>th</sup> March 1997. To estimate the strength of the flux in 2014, it is necessary to consider the nuclear decay through time assiciated to the Cesium source whose half-life is well known ( $t_{1/2} = (30.05 \pm 0.08)$  y). The GIF tests where done in between the 20<sup>th</sup> and the 31<sup>st</sup> of August 2014, i.e. at a time  $t = (17.47 \pm 0.02)$  y resulting in an attenuation of the activity from 740 GBq in 1997 to 494 GBq in 2014.

557

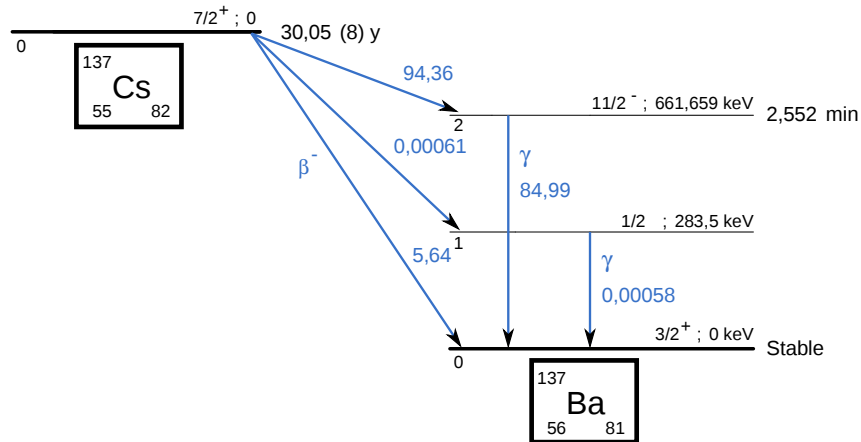


Figure 5.4:  $^{137}\text{Cs}$  decays by  $\beta^-$  emission to the ground state of  $^{137}\text{Ba}$  ( $BR = 5.64\%$ ) and via the 662 keV isomeric level of  $^{137}\text{Ba}$  ( $BR = 94.36\%$ ) whose half-life is 2.55 min.

### 5.1.1.2 GIF++

The new Gamma Irradiation Facility (GIF++), located in the SPS North Area at the downstream end of the H4 test beam, has replaced its predecessor during LS1 and has been operational since spring 2015 [7]. Like GIF, GIF++ features a  $^{137}\text{Cs}$  source of 662 keV gamma photons, their fluence being controlled with a set of filters of various attenuation factors. The source provides two separated large irradiation areas for testing several full-size muon detectors with continuous homogeneous irradiation, as presented in Figure 5.5.

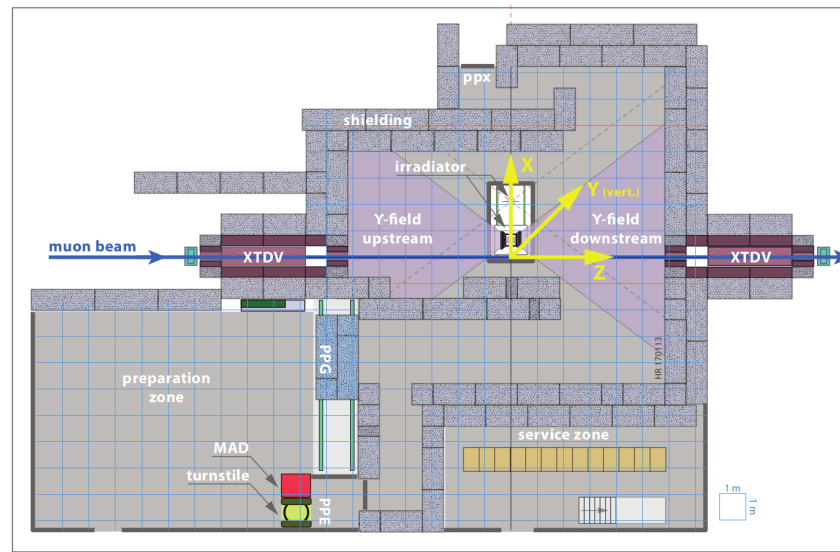


Figure 5.5: Floor plan of the GIF++ facility. When the facility downstream of the GIF++ takes electron beam, a beam pipe is installed along the beam line ( $z$ -axis). The irradiator can be displaced laterally (its center moves from  $x = 0.65 \text{ m}$  to  $2.15 \text{ m}$ ), to increase the distance to the beam pipe.

566 The source activity was measured to be about 13.5 TBq in March 2016. The photon flux being  
 567 far greater than HL-LHC expectations, GIF++ provides an excellent facility for accelerated aging  
 568 tests of muon detectors.

569

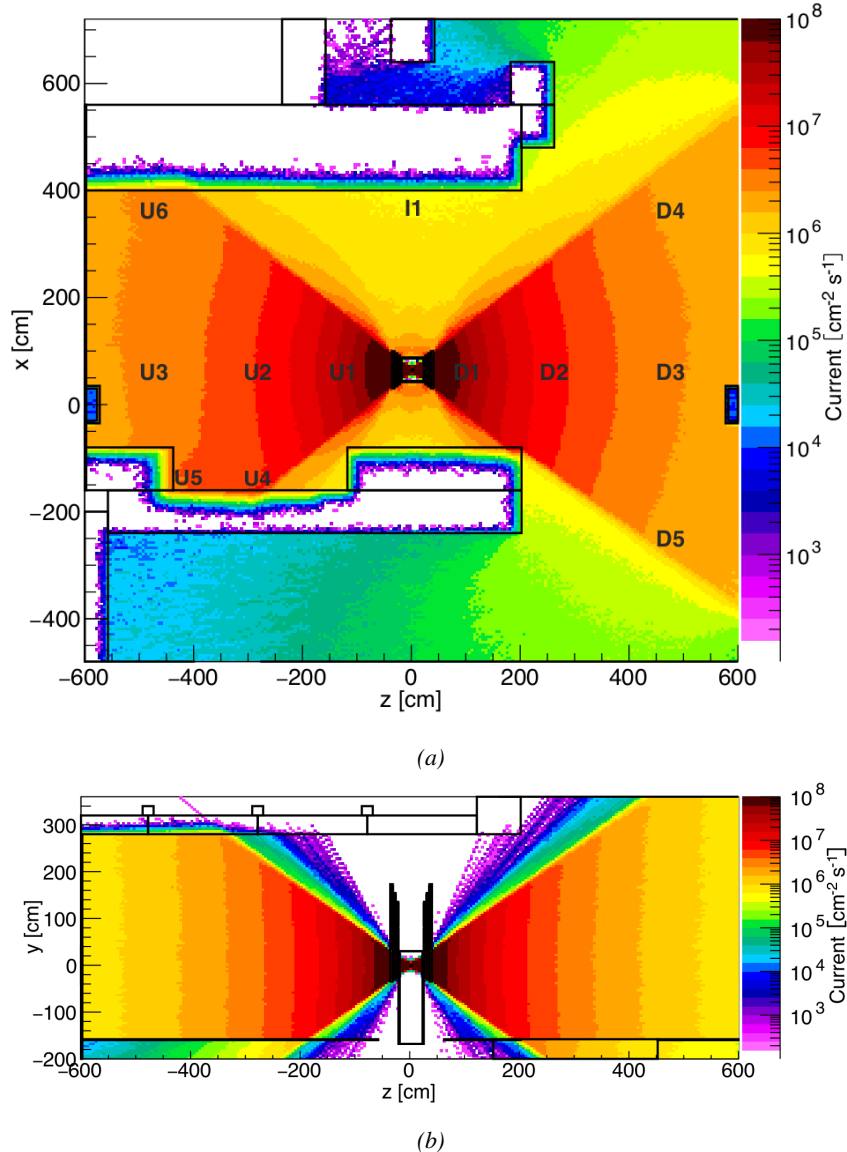


Figure 5.6: Simulated unattenuated current of photons in the xz plane (Figure 5.6a) and yz plane (Figure 5.6b) through the source at  $x = 0.65$  m and  $y = 0$  m. With angular correction filters, the current of 662 keV photons is made uniform in xy planes.

570 The source is situated in the muon beam line with the muon beam being available a few times a  
 571 year. The H4 beam, composed of muons with a momentum of about 150 GeV/c, passes through the  
 572 GIF++ zone and is used to study the performance of the detectors. Its flux is of 104 particles/ $\text{s}/\text{cm}^2$

573 focused in an area similar to  $10 \times 10 \text{ cm}^2$ . Therefore, with properly adjusted filters, one can imitate  
 574 the HL-LHC background and study the performance of muon detectors with their trigger/readout  
 575 electronics in HL-LHC environment.

576

## 577 5.2 Preliminary tests at GIF

### 578 5.2.1 Resistive Plate Chamber test setup

579 During summer 2014, preliminary tests have been conducted in the GIF area on a newly produced  
 580 RE4/2 chamber labelled RE-4-2-BARC-161. This chamber has been placed into a trolley covered  
 581 with a tent. The position of the RPC inside the tent and of the tent related to the source is described  
 582 in Figure 5.7. To test this CMS RPC, three different absorber settings were used. First of all,  
 583 measurements were done with fully opened source. Then, to complete this preliminary study, the  
 584 gamma flux has been attenuated from a factor 2 and a factor 5. The expected gamma flux at the level  
 585 of our detector will be discussed in subsection ??.

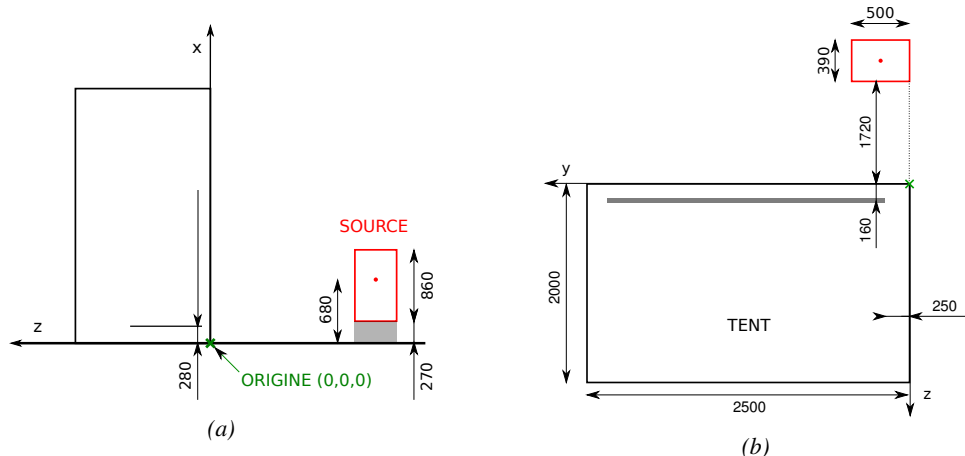
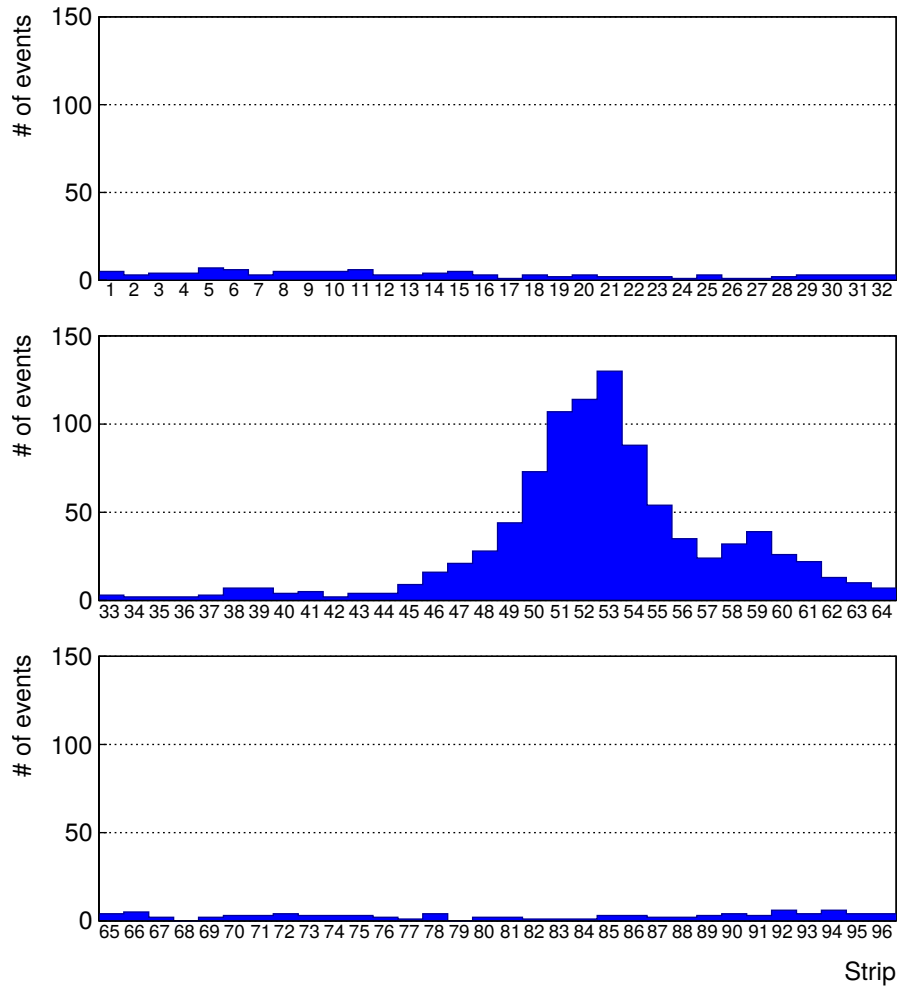


Figure 5.7: Description of the RPC setup. Dimensions are given in mm. A tent containing RPCs is placed at 1720 mm from the source container. The source is situated in the center of the container. RE-4-2-BARC-161 chamber is 160 mm inside the tent. This way, the distance between the source and the chambers plan is 2060 mm. Figure 5.7a provides a side view of the setup in the xz plane while Figure 5.7b shows a top view in the yz plane.



*Figure 5.8: RE-4-2-BARC-161 chamber is inside the tent as described in Figure 5.7. In the top right, the two scintillators used as trigger can be seen. This trigger system has an inclination of 10° relative to horizontal and is placed above half-partition B2 of the RPCs. PMT electronics are shielded thanks to lead blocks placed in order to protect them without stopping photons from going through the scintillators and the chamber.*

586 At the time of the tests, the beam not being operational anymore, a trigger composed of 2  
 587 plastic scintillators has been placed in front of the setup with an inclination of 10 deg with respect to  
 588 the detector plane in order to look at cosmic muons. Using this particular trigger layout, shown on  
 589 Figure 5.8, leads to a cosmic muon hit distribution into the chamber similar to the one in Figure 5.9.  
 590 Measured without gamma irradiation, two peaks can be seen on the profil of partition B, centered  
 591 on strips 52 and 59. Section ?? will help us understand that these two peaks are due respectively to  
 592 forward and backward coming cosmic particles where forward coming particles are first detected by  
 593 the scintillators and then the RPC while the backward coming muons are first detected in the RPC.



*Figure 5.9: Hit distributions over all 3 partitions of RE-4-2-BARC-161 chamber is showed on these plots. Top, middle and bottom figures respectively correspond to partitions A, B, and C. These plots show that some events still occur in other half-partitions than B2, which corresponds to strips 49 to 64, in front of which the trigger is placed, contributing to the inefficiency of detection of cosmic muons. In the case of partitions A and C, the very low amount of data can be interpreted as noise. On the other hand, it is clear that a little portion of muons reach the half-partition B1, corresponding to strips 33 to 48.*

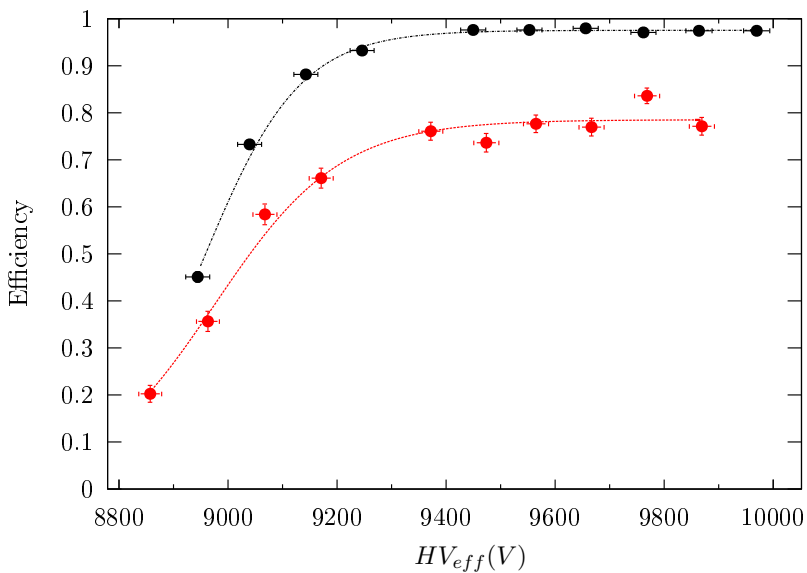
### 594 5.2.2 Data Acquisition

### 595 5.2.3 Geometrical acceptance of the setup layout to cosmic muons

596 In order to profit from a constant gamma irradiation, the detectors inside of the GIF bunker need  
 597 to be placed in a plane orthogonal to the beam line. The muon beam that used to be available was  
 598 meant to test the performance of detectors under test. This beam not being active anymore, another  
 599 solution to test detector performance had to be used. Thus, it has been decided to use cosmic muons  
 600 detected through a telescope composed of two scintillators. Lead blocks were used as shielding to

601 protect the photomultipliers from gammas as can be seen from Figure 5.8.

602 An inclination has been given to the cosmic telescope to maximize the muon flux. A good com-  
 603 promise had to be found between good enough muon flux and narrow enough hit distribution to  
 604 be sure to contain all the events into only one half partitions as required from the limited available  
 605 readout hardware. Nevertheless, a consequence of the misplaced trigger, that can be seen as a loss  
 606 of events in half-partition B1 in Figure 5.9, is an inefficiency. Nevertheless, the inefficiency of ap-  
 607 proximately 20 % highlighted in Figure 5.10 by comparing the performance of chamber BARC-161  
 608 in 904 and at GIF without irradiation seems too important to be explained only by the geometri-  
 609 cal acceptance of the setup itself. Simulations have been conducted to show how the setup brings  
 610 inefficiency.



5.10: Results are derived from data taken on half-partition B2 only. On the 18<sup>th</sup> of June 2014, data has been taken on chamber RE-2-BARC-161 at building 904 (Prevessin Site) with cosmic muons providing us a reference efficiency plateau of  $(97.54 \pm 0.15)\%$  represented by a black curve. A similar measurement has been done at GIF on the 21<sup>st</sup> of July with the same chamber giving a plateau of  $(78.52 \pm 0.94)\%$  represented by a red curve.

### 611 5.2.3.1 Description of the simulation layout

612 The layout of GIF setup has been reproduced and incorporated into a Monte Carlo (MC) simulation  
 613 to study the influence of the disposition of the telescope on the final distribution measured by the  
 614 RPC. A 3D view of the simulated layout is given into Figure 5.11. Muons are generated randomly  
 615 in a horizontal plane located at a height corresponding to the lowest point of the PMTs. This way,  
 616 the needed size of the plane in order to simulate events happening at very big azimuthal angles (i.e.  
 617  $\theta \approx \pi$ ) can be kept relatively small. The muon flux is designed to follow the usual  $\cos^2\theta$  distribution  
 618 for cosmic particle. The goal of the simulation is to look at muons that pass through the muon  
 619 telescope composed of the two scintillators and define their distribution onto the RPC plane. During  
 620 the reconstruction, the RPC plane is then divided into its strips and each muon track is assigned to a  
 621 strip.

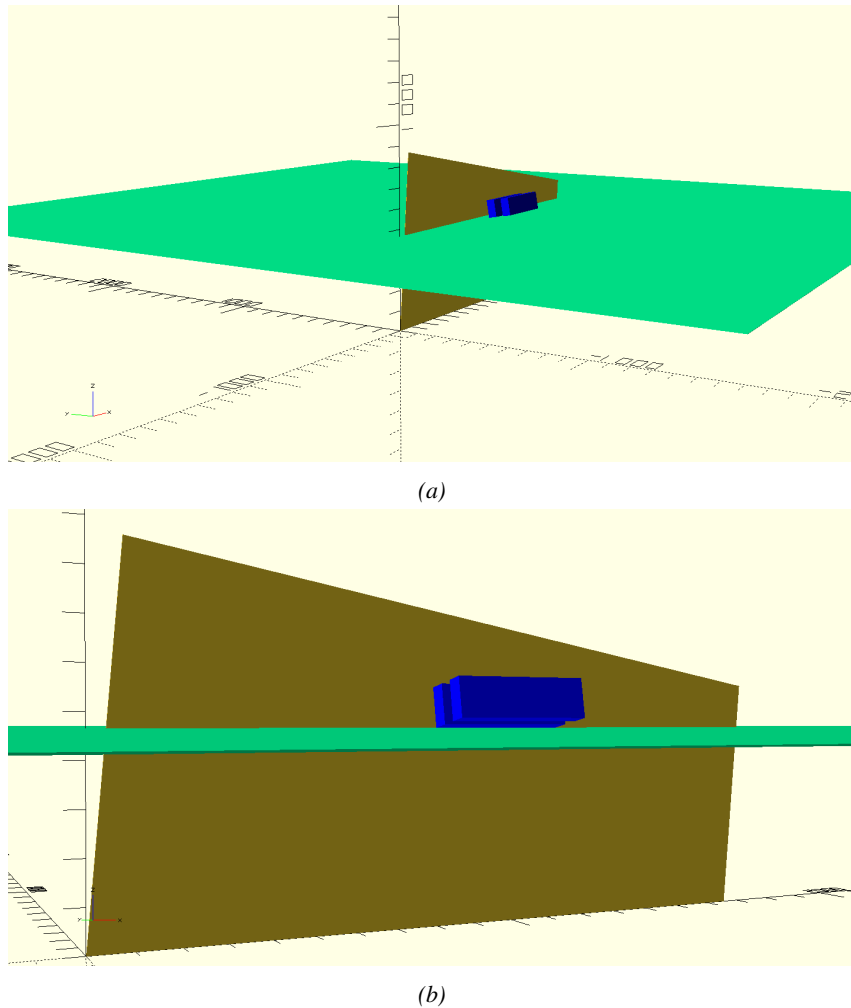


*Figure 5.11: Representation of the layout used for the simulations of the test setup. The RPC is represented as a yellow trapezoid while the two scintillators as blue cuboids looking at the sky. A green plane corresponds to the muon generation plane within the simulation. Figure 5.7a shows a global view of the simulated setup. Figure 5.7b shows a zoomed view that allows to see the 2 scintillators as well as the full RPC plane.*

622 In order to further refine the quality of the simulation and understand deeper the results the  
 623 dependance of the distribution has been studied for a range of telescope inclinations. Moreover,  
 624 the threshold applied on the PMT signals has been included into the simulation in the form of a  
 625 cut. In the approximation of uniform scintillators, it has been considered that the threshold can be  
 626 understood as the minimum distance particles need to travel through the scintillating material to give  
 627 a strong enough signal. Particles that travel a distance smaller than the set "threshold" are thus not  
 628 detected by the telescope and cannot trigger the data taking. Finally, the FEE threshold also has  
 629 been considered in a similar way. The mean momentum of horizontal cosmic rays is higher than  
 630 those of vertical ones but the stopping power of matter for momenta ranging from 1 GeV to 1 TeV  
 631 stays comparable. It is then possible to assume that the mean number of primary  $e^-/ion$  pairs per  
 632 unit length will stay similar and thus, depending on the applied discriminator threshold, muons with

633 the shortest path through the gas volume will deposit less charge and induce a smaller signal on the  
 634 pick-up strips that could eventually not be detected. These two thresholds also restrain the overall  
 635 geometrical acceptance of the system.

636 **5.2.3.2 Simulation procedure**

637 The simulation software has been designed using C++ and the output data is saved into ROOT  
 638 histograms. Simulations start for a threshold  $T_{scint}$  varying in a range from 0 to 45 mm in steps  
 639 of 5 mm, where  $T_{scint} = 0$  mm corresponds to the case where there isn't any threshold apply on  
 640 the input signal while  $T_{scint} = 45$  mm, which is the scintillator thickness, is the case where muons  
 641 cannot arrive orthogonally onto the scintillator surface. For a given  $T_{scint}$ , a set of RPC thresholds  
 642 are considered. The RPC threshold,  $T_{RPC}$  varies from 2 mm, the thickness of the gas volume, to  
 643 3 mm in steps of 0.25 mm. For each  $(T_{scint}; T_{RPC})$  pair,  $N_\mu = 10^8$  muons are randomly generated  
 644 inside the muon plane described in the previous paragraph with an azimuthal angle  $\theta$  chosen to follow  
 645 a  $\cos^2\theta$  distribution.

646 Planes are associated to each surface of the scintillators. Knowing muon position into the muon  
 647 plane and its direction allows us, by assuming that muons travel in a straight line, to compute the  
 648 intersection of the muon track with these planes. Applying conditions to the limits of the surfaces  
 649 of the scintillator faces then gives us an answer to whether or not the muon passed through the  
 650 scintillators. In the case the muon has indeed passed through the telescope, the path through each  
 651 scintillator is computed and muons whose path was shorter than  $T_{scint}$  are rejected and are thus  
 652 considered as having not interacted with the setup.

653 On the contrary, if the muon is labeled as good, its position within the RPC plane is computed  
 654 and the corresponding strip, determined by geometrical tests in the case the distance through the  
 655 gas volume was enough not to be rejected because of  $T_{RPC}$ , gets a hit and several histograms  
 656 are filled in order to keep track of the generation point on the muon plane, the intersection points  
 657 of the reconstructed muons within the telescope, or on the RPC plane, the path traveled through  
 658 each individual scintillator or the gas volume, as well as other histograms. Moreover, muons fill  
 659 different histograms whether they are forward or backward coming muons. They are discriminated  
 660 according to their direction components. When a muon is generated, an  $(x, y, z)$  position is assigned  
 661 into the muon plane as well as a  $(\theta; \phi)$  pair that gives us the direction it's coming from. This way,  
 662 muons satisfying the condition  $0 \leq \phi < \pi$  are designated as backward coming muons while muons  
 663 satisfying  $\pi \leq \phi < 2\pi$  as forward coming muons.

664 This simulation is then repeated for different telescope inclinations ranging in between 4 and  $20^\circ$   
 665 and varying in steps of  $2^\circ$ . Due to this inclination and to the vertical position of the detector under  
 666 test, the muon distribution reconstructed in the detector plane is asymmetrical. The choice as been  
 667 made to chose a skew distribution formula to fit the data built as the multiplication of gaussian and  
 668 sigmoidal curves together. A typical gaussian formula is given as 5.1 and has three free parameters  
 669 as  $A_g$ , its amplitude,  $\bar{x}$ , its mean value and  $\sigma$ , its root mean square. Sigmoidal curves as given by  
 670 formula 5.2 are functions converging to 0 and  $A_s$  as  $x$  diverges. The inflection point is given as  $x_i$   
 671 and  $\lambda$  is proportional to the slope at  $x = x_i$ . In the limit where  $\lambda \rightarrow \infty$ , the sigmoid becomes a  
 672 step function.

$$g(x) = A_g e^{-\frac{(x-\bar{x})^2}{2\sigma^2}} \quad (5.1)$$

$$s(x) = \frac{A_s}{1 + e^{-\lambda(x-x_i)}} \quad (5.2)$$

673 Finally, a possible representation of a skew distribution is given by formula 5.3 and is the product  
 674 of 5.1 and 5.2. Naturally, here  $A_{sk} = A_g \times A_s$  and represents the theoretical maximum in the limit  
 675 where the skew tends to a gaussian function.

$$sk(x) = g(x) \times s(x) = A_{sk} \frac{e^{\frac{-(x-\bar{x})^2}{2\sigma^2}}}{1 + e^{-\lambda(x-x_i)}} \quad (5.3)$$

676 **5.2.3.3 Results**

677 **Influence of  $T_{scint}$  on the muon distribution**

678 **Influence of  $T_{RPC}$  on the muon distribution**

679 **Influence of the telescope inclination on the muon distribution**

680 **Comparison to data taken at GIF without irradiation**

681 **5.2.4 Photon flux at GIF**

682 **5.2.4.1 Expectations from simulations**

683 In order to understand and evaluate the  $\gamma$  flux in the GIF area, simulations had been conducted in  
 684 1999 and published by S. Agosteo et al [6]. Table 5.1 presented in this article gives us the  $\gamma$  flux  
 685 for different distances  $D$  to the source. This simulation was done using GEANT and a Monte Carlo  
 686 N-Particle (MCNP) transport code, and the flux  $F$  is given in number of  $\gamma$  per unit area and unit time  
 687 along with the estimated error from these packages expressed in %.

Nominal ABS	Photon flux $F$ [ $s^{-1}cm^{-2}$ ]			
	at $D = 50$ cm	at $D = 155$ cm	at $D = 300$ cm	at $D = 400$ cm
1	$0.12 \cdot 10^8 \pm 0.2\%$	$0.14 \cdot 10^7 \pm 0.5\%$	$0.45 \cdot 10^6 \pm 0.5\%$	$0.28 \cdot 10^6 \pm 0.5\%$
2	$0.68 \cdot 10^7 \pm 0.3\%$	$0.80 \cdot 10^6 \pm 0.8\%$	$0.25 \cdot 10^6 \pm 0.8\%$	$0.16 \cdot 10^6 \pm 0.6\%$
5	$0.31 \cdot 10^7 \pm 0.4\%$	$0.36 \cdot 10^6 \pm 1.2\%$	$0.11 \cdot 10^6 \pm 1.2\%$	$0.70 \cdot 10^5 \pm 0.9\%$

Table 5.1: Total photon flux ( $E\gamma \leq 662$  keV) with statistical error predicted considering a  $^{137}Cs$  activity of 740 GBq at different values of the distance  $D$  to the source along the  $x$ -axis of irradiation field [6].

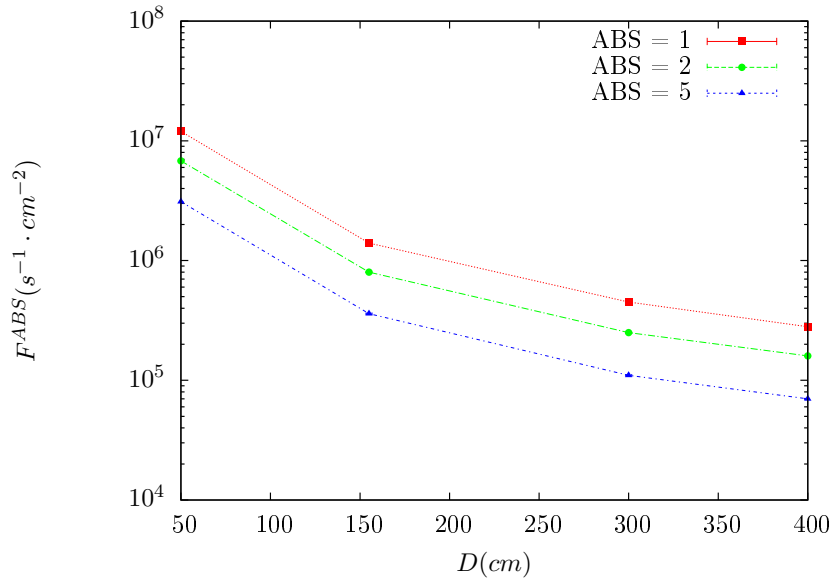


Figure 5.12:  $\gamma$  flux  $F(D)$  is plot using values from table 5.1. As expected, the plot shows similar attenuation behaviours with increasing distance for each absorption factors.

The simulation doesn't directly provides us with an estimated flux at the level of our RPC. First of all, it is needed to extract the value of the flux from the available data contained in the original paper and then to estimate the flux in 2014 at the time the experimentation took place. Figure 5.12 that contains the data from Table 5.1. In the case of a pointlike source emitting isotropic and homogeneous gamma radiations, the gamma flux  $F$  at a distance  $D$  to the source with respect to a reference point situated at  $D_0$  where a known flux  $F_0$  is measured will be expressed like in Equation 5.4, assuming that the flux decreases as  $1/D^2$ , where  $c$  is a fitting factor.

$$F^{ABS} = F_0^{ABS} \times \left( \frac{cD_0}{D} \right)^2 \quad (5.4)$$

By rewriting Equation 5.4, it comes that :

$$c = \frac{D}{D_0} \sqrt{\frac{F^{ABS}}{F_0^{ABS}}} \quad (5.5)$$

$$\Delta c = \frac{c}{2} \left( \frac{\Delta F^{ABS}}{F^{ABS}} + \frac{\Delta F_0^{ABS}}{F_0^{ABS}} \right) \quad (5.6)$$

Finally, using Equation 5.5 and the data in Table 5.1 with  $D_0 = 50$  cm as reference point, we can build Table 5.2. It is interesting to note that  $c$  for each value of  $D$  doesn't depend on the absorption factor.

Nominal ABS	Correction factor $c$		
	at $D = 155$ cm	at $D = 300$ cm	at $D = 400$ cm
1	$1.059 \pm 0.70\%$	$1.162 \pm 0.70\%$	$1.222 \pm 0.70\%$
2	$1.063 \pm 1.10\%$	$1.150 \pm 1.10\%$	$1.227 \pm 0.90\%$
5	$1.056 \pm 1.60\%$	$1.130 \pm 1.60\%$	$1.202 \pm 1.30\%$

Table 5.2: Correction factor  $c$  is computed thanks to formulae 5.5 taking as reference  $D_0 = 50$  cm and the associated flux  $F_0^{ABS}$  for each absorption factor available in table 5.1.

699 For the range of  $D/D_0$  values available, it is possible to use a simple linear fit to get the evolution  
700 of  $c$ . The linear fit will then use only 2 free parameters,  $a$  and  $b$ , as written in Equation 5.7. This gives  
701 us the results showed in Figure 5.13. Figure 5.13b confirms that using only a linear fit to extract  $c$  is  
702 enough as the evolution of the rate that can be obtained superimposes well on the simulation points.

$$c \left( \frac{D}{D_0} \right) = a \frac{D}{D_0} + b \quad (5.7)$$

$$F^{ABS} = F_0^{ABS} \left( a + \frac{bD_0}{D} \right)^2 \quad (5.8)$$

$$\Delta F^{ABS} = F^{ABS} \left[ \frac{\Delta F_0^{ABS}}{F_0^{ABS}} + 2 \frac{\Delta a + \Delta b \frac{D_0}{D}}{a + \frac{bD_0}{D}} \right] \quad (5.9)$$

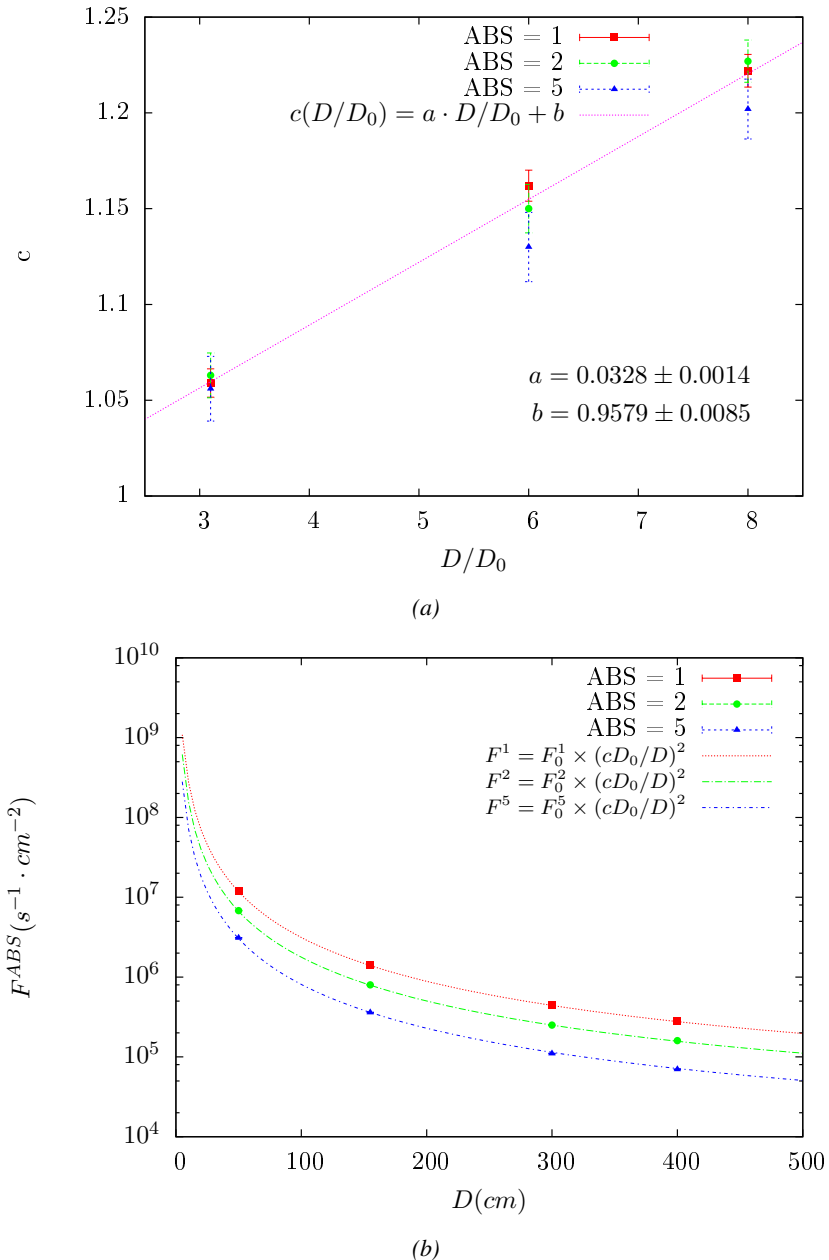


Figure 5.13: Figure 5.13a shows the linear approximation fit done via formulae 5.7 on data from table 5.2. Figure 5.13b shows a comparison of this model with the simulated flux using  $a$  and  $b$  given in figure 5.13a in formulae 5.4 and the reference value  $D_0 = 50\text{cm}$  and the associated flux for each absorption factor  $F_0^{ABS}$  from table 5.1

In the case of the 2014 GIF tests, the RPC plane is located at a distance  $D = 206\text{ cm}$  to the source.  
 Moreover, to estimate the strength of the flux in 2014, it is necessary to consider the nuclear decay through time associated to the Cesium source whose half-life is well known ( $t_{1/2} = (30.05 \pm 0.08)\text{ y}$ ).  
 The very first source activity measurement has been done on the 5<sup>th</sup> of March 1997 while the GIF

707 tests where done in between the 20<sup>th</sup> and the 31<sup>st</sup> of August 2014, i.e. at a time  $t = (17.47 \pm 0.02)$  y  
 708 resulting in an attenuation of the activity from 740 GBq in 1997 to 494 GBq in 2014. All the needed  
 709 information to extrapolate the flux through our detector in 2014 has now been assembled, leading  
 710 to the Table 5.3. It is interesting to note that for a common RPC sensitivity to  $\gamma$  of  $2 \cdot 10^{-3}$ , the  
 711 order of magnitude of the estimated hit rate per unit area is of the order of the kHz for the fully  
 712 opened source. Moreover, taking profit of the two working absorbers, it will be possible to scan  
 713 background rates at 0 Hz,  $\sim 300$  Hz as well as  $\sim 600$  Hz. Without source, a good estimate of the  
 714 intrinsic performance will be available. Then at 300 Hz, the goal will be to show that the detectors  
 715 fulfill the performance certification of CMS RPCs. Then a first idea of the performance of the  
 716 detectors at higher background will be provided with absorption factors 2 ( $\sim 600$  Hz) and 1 (no  
 717 absorption). *[Here I will also put a reference to the plot showing the estimated background rate at  
 718 the level of RE3/1 in the case of HL-LHC but this one being in another chapter, I will do it later.]*

Nominal ABS	Photon flux $F$ [ $s^{-1}cm^{-2}$ ]			Hit rate/unit area [ $Hz cm^{-2}$ ] at $D^{2014} = 206$ cm
	at $D_0^{1997} = 50$ cm	at $D_0^{1997} = 206$ cm	at $D^{2014} = 206$ cm	
1	$0.12 \cdot 10^8 \pm 0.2\%$	$0.84 \cdot 10^6 \pm 0.3\%$	$0.56 \cdot 10^6 \pm 0.3\%$	$1129 \pm 32$
2	$0.68 \cdot 10^7 \pm 0.3\%$	$0.48 \cdot 10^6 \pm 0.3\%$	$0.32 \cdot 10^6 \pm 0.3\%$	$640 \pm 19$
5	$0.31 \cdot 10^7 \pm 0.4\%$	$0.22 \cdot 10^6 \pm 0.3\%$	$0.15 \cdot 10^6 \pm 0.3\%$	$292 \pm 9$

Table 5.3: The data at  $D_0$  in 1997 is taken from [6]. In a second step, using Equations 5.8 and 5.9, the flux at  $D$  can be estimated in 1997. Then, taking into account the attenuation of the source activity, the flux at  $D$  can be estimated at the time of the tests in GIF in 2014. Finally, assuming a sensitivity of the RPC to  $\gamma$   $s = 2 \cdot 10^{-3}$ , an estimation of the hit rate per unit area is obtained.

<sup>719</sup> **5.2.4.2 Dose measurements**

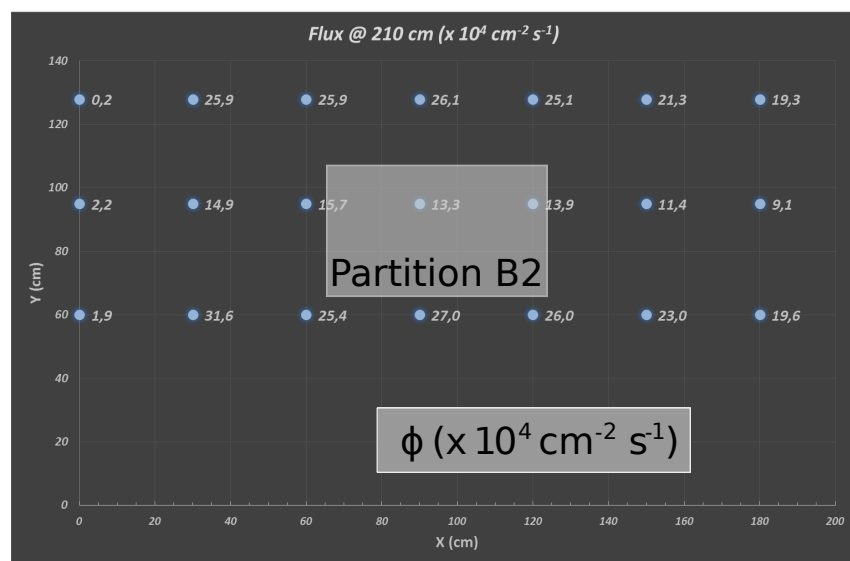


Figure 5.14: Dose measurements has been done in a plane corresponding to the tents front side. This plan is 1900 mm away from the source. As explained in the first chapter, a lens-shaped lead filter provides a uniform photon flux in the vertical plan orthogonal to the beam direction. If the second line of measured fluxes is not taken into account because of lower values due to experimental equipments in the way between the source and the tent, the uniformity of the flux is well showed by the results.

<sup>720</sup> **5.2.5 Results and discussions**

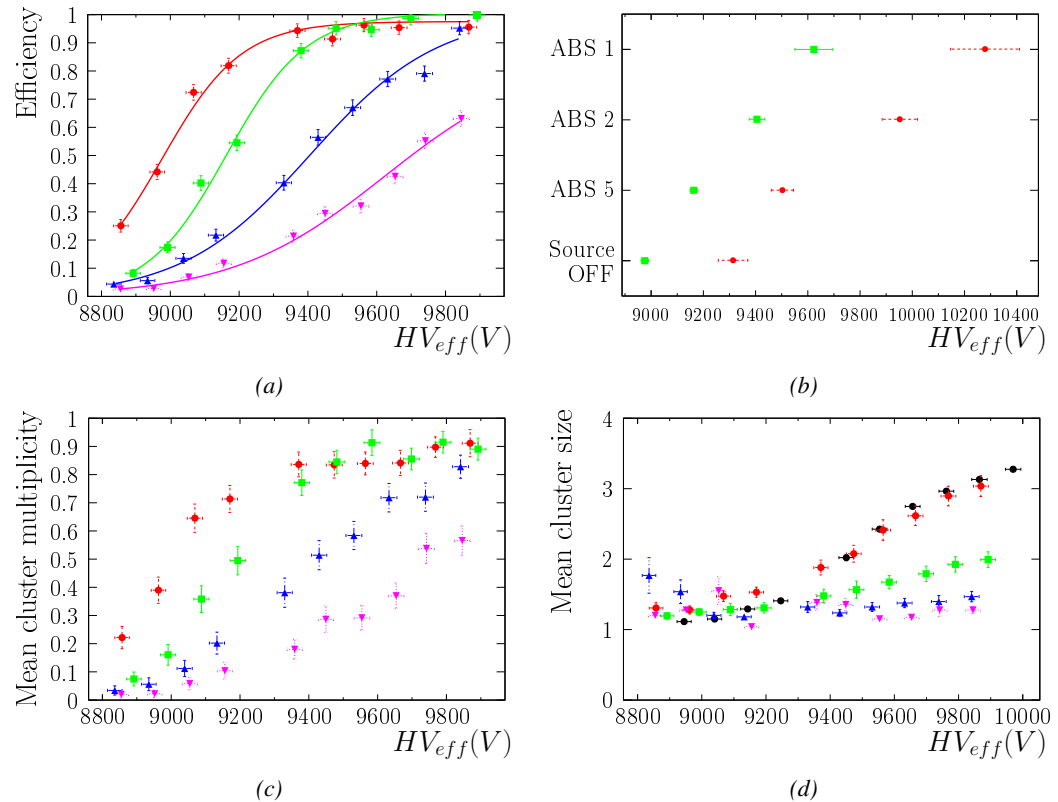


Figure 5.15

**721 5.3 Longevity tests at GIF++**

722 Longevity studies imply a monitoring of the performance of the detectors probed using a high inten-  
723 sity muon beam in a irradiated environment by periodically measuring their rate capability, the dark  
724 current running through them and the bulk resistivity of the Bakelite composing their electrodes.  
725 GIF++, with its very intense  $^{137}\text{Cs}$  source, provides the perfect environment to perform such kind  
726 of tests. Assuming a maximum acceleration factor of 3, it is expected to accumulate the equivalent  
727 charge in 1.7 years.

728 As the maximum background is found in the endcap, the choice naturally was made to focus the  
729 GIF++ longevity studies on endcap chambers. Most of the RPC system was installed in 2007. Nev-  
730 ertheless, the large chambers in the fourth endcap (RE4/2 and RE4/3) have been installed during  
731 LS1 in 2014. The Bakelite of these two different productions having different properties, four spare  
732 chambers of the present system were selected, two RE2,3/2 spares and two RE4/2 spares. Having  
733 two chambers of each type allows to always keep one of them non irradiated as reference, the per-  
734 formance evolution of the irradiated chamber being then compared through time to the performance  
735 of the non irradiated one.

736 The performance of the detectors under different level of irradiation is measured periodically dur-  
737 ing dedicated test beam periods using the H4 muon beam. In between these test beam periods, the  
738 two RE2,3/2 and RE4/2 chambers selected for this study are irradiated by the  $^{137}\text{Cs}$  source in order  
739 to accumulate charge and the gamma background is monitored, as well as the currents. The two  
740 remaining chambers are kept non-irradiated as reference detectors. Due to the limited gas flow in  
741 GIF++, the RE4 chamber remained non-irradiated until end of November 2016 where a new mass  
742 flow controller has been installed allowing for bigger volumes of gas to flow in the system.

743 Figures 5.16 and 5.17 give us for different test beam periods, and thus for increasing integrated  
744 charge through time, a comparison of the maximum efficiency, obtained using a sigmoid-like func-  
745 tion, and of the working point of both irradiated and non irradiated chambers [8]. No aging is yet to  
746 see from this data, the shifts in  $\gamma$  rate per unit area in between irradiated and non irradiated detec-  
747 tors and RE2 and RE4 types being easily explained by a difference of sensitivity due to the various  
748 Bakelite resistivities of the HPL electrodes used for the electrode production.

749 Collecting performance data at each test beam period allows us to extrapolate the maximum effi-  
750 ciency for a background hit rate of  $300\text{ Hz}/\text{cm}^2$  corresponding to the expected HL-LHC conditions.  
751 Aging effects could emerge from a loss of efficiency with increasing integrated charge over time,  
752 thus Figure 5.18 helps us understand such degradation of the performance of irradiated detectors in  
753 comparison with non irradiated ones. The final answer for an eventual loss of efficiency is given in  
754 Figure 5.19 by comparing for both irradiated and non irradiated detectors the efficiency sigmoids  
755 before and after the longevity study. Moreover, to complete the performance information, the Bake-  
756 lite resistivity is regularly measured thanks to  $Ag$  scans (Figure 5.20) and the noise rate is monitored  
757 weekly during irradiation periods (Figure 5.21). At the end of 2016, no signs of aging were observed  
758 and further investigation is needed to get closer to the final integrated charge requirements proposed  
759 for the longevity study of the present CMS RPC sub-system.

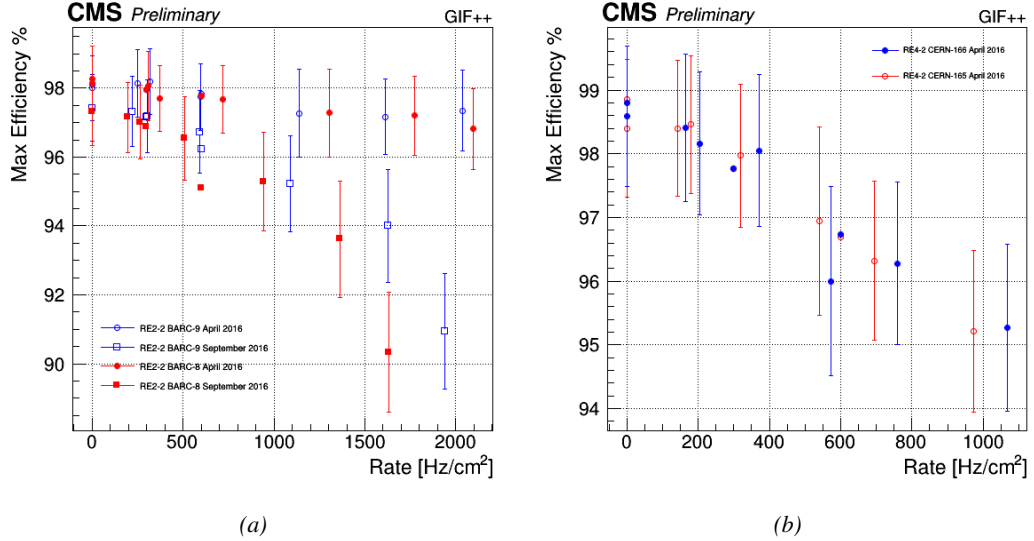


Figure 5.16: Evolution of the maximum efficiency for RE2 (5.16a) and RE4 (5.16b) chambers with increasing extrapolated  $\gamma$  rate per unit area at working point. Both irradiated (blue) and non irradiated (red) chambers are shown.

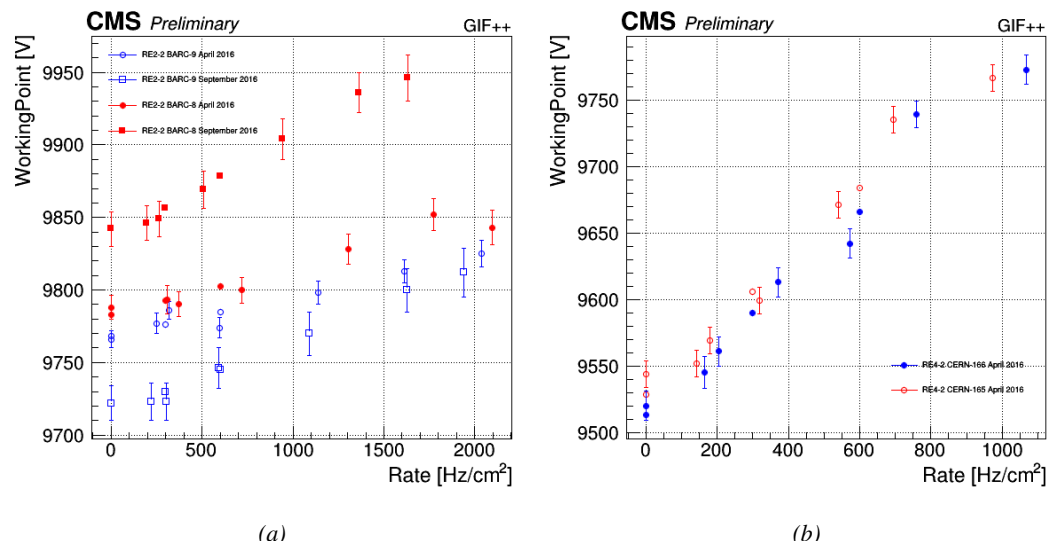


Figure 5.17: Evolution of the working point for RE2 (5.17a) and RE4 (5.17b) with increasing extrapolated  $\gamma$  rate per unit area at working point. Both irradiated (blue) and non irradiated (red) chambers are shown.

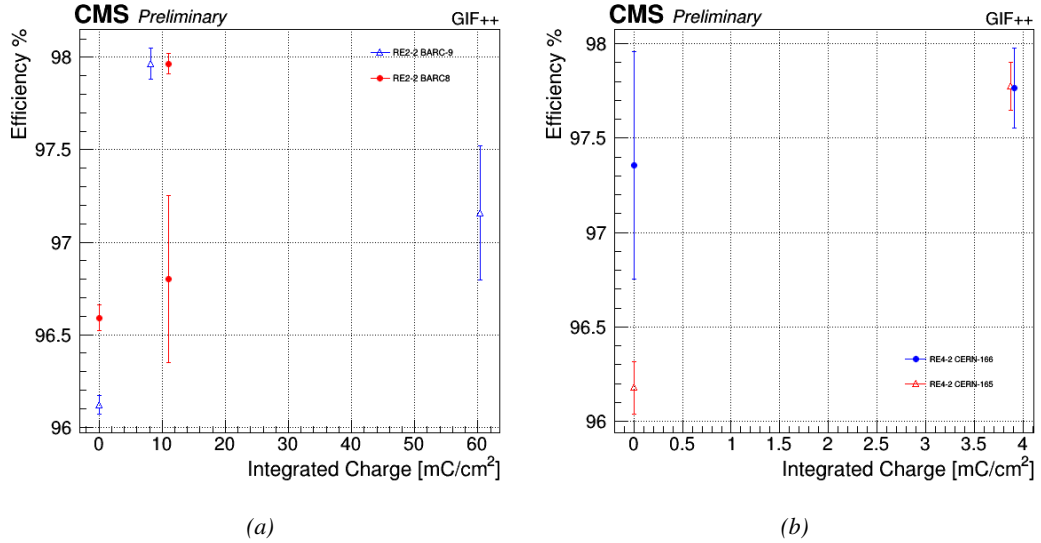


Figure 5.18: Evolution of the maximum efficiency at HL-LHC conditions, i.e. a background hit rate per unit area of  $300 \text{ Hz}/\text{cm}^2$ , with increasing integrated charge for RE2 (5.18a) and RE4 (5.18b) detectors. Both irradiated (blue) and non irradiated (red) chambers are shown. The integrated charge for non irradiated detectors is recorded during test beam periods and stays small with respect to the charge accumulated in irradiated chambers.

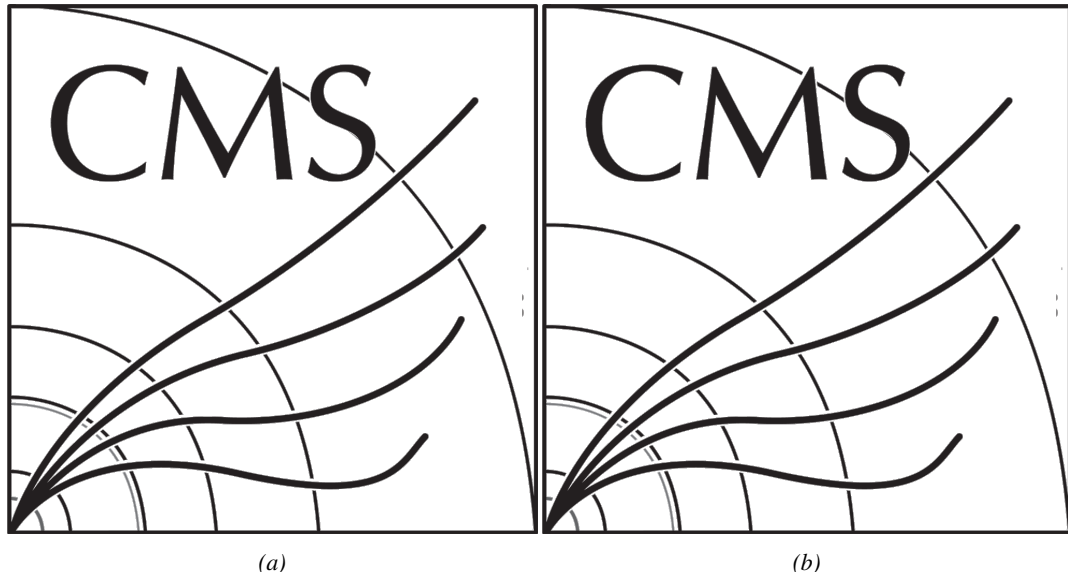


Figure 5.19: Comparison of the efficiency sigmoid before (triangles) and after (circles) irradiation for RE2 (5.19a) and RE4 (5.19b) detectors. Both irradiated (blue) and non irradiated (red) chambers are shown.

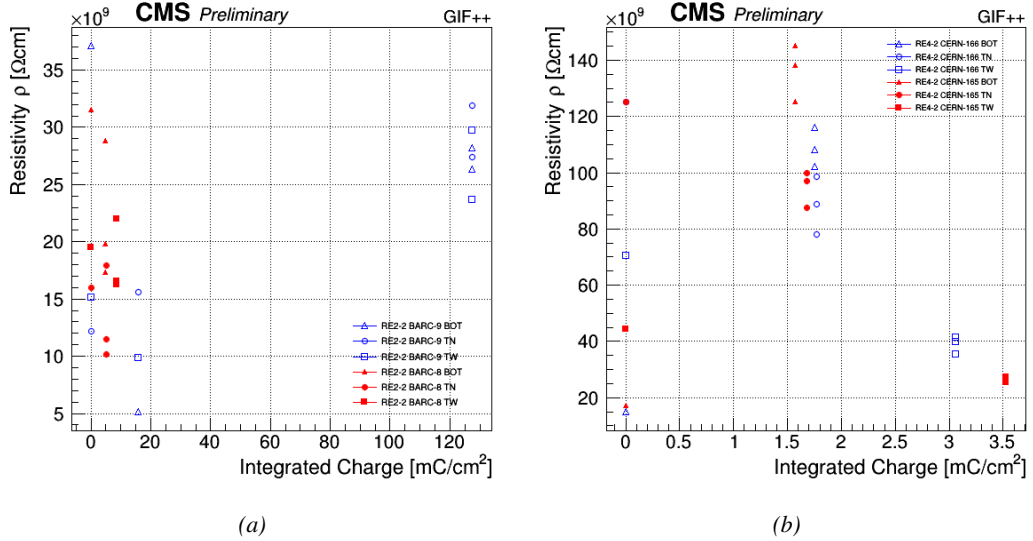


Figure 5.20: Evolution of the Bakelite resistivity for RE2 (5.20a) and RE4 (5.20b) detectors. Both irradiated (blue) and non-irradiated (red) chambers are shown.

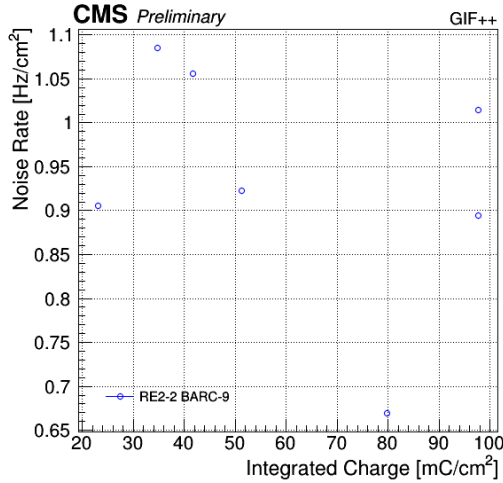


Figure 5.21: Evolution of the noise rate per unit area for the irradiated chamber RE2-2-BARC-9 only.

### 5.3.1 Description of the Data Acquisition

For the longevity studies, four spare chambers of the present system are used. Two spare RPCs of the RE2,3 stations as well as two spare RPCs from the new RE4 stations have been mounted in a Trolley. Six RE4 gaps are also placed in the trolley. The trolley is placed inside the GIFT++ in the upstream region of the bunker, taking the cesium source as a reference. The trolley is oriented for the detection surface of the chambers to be orthogonal to the beam line. The system can be moved along the orthogonal plane in order to have the beam in all  $\eta$ -partitions. For the aging the trolley is

768 moved outside the beam line and is placed in a distance of 5.2 m to the source, which irradiates the  
 769 bunker using an attenuation filter of 2.2 which corresponds to a fluence of  $10^7 \text{ gamma/cm}^2$ .

770 During GIF++ operation, the data collected can be divided into different categories as several  
 771 parameters are monitored in addition to the usual RPC performance data. On one hand, to know  
 772 the performance of a chamber, it is need to measure its efficiency and to know the background  
 773 conditions in which it is operated. To do this, the hit signals from the chamber are recorded and  
 774 stored in a ROOT file via a Data Acquisition (DAQ) software. On the other hand, it is also very  
 775 important to monitor parameters such as environmental pressure and temperature, gas temperature  
 776 and humidity, RPC HV, LV, and currents, or even source and beam status. This is done through the  
 777 GIF++ web Detector Control Software (DCS) that stores this information in a database.

778 Two different types of tests are conducted on RPCs via the DAQ. Indeed, the performance of the  
 779 detectors is measured periodically during dedicated test beam periods using the H4 muon beam. In  
 780 between these test beam periods, when the beam is not available, the chambers are irradiated by the  
 781  $^{137}\text{Cs}$  in order to accumulate deposited charge and the gamma background is measured.

782 RPCs under test are connected through LVDS cables to V1190A Time-to-Digital Converter  
 783 (TDC) modules manufactured by CAEN. These modules, located in the rack area outside of the  
 784 bunker, get the logic signals sent by the chambers and save them into their buffers. Due to the  
 785 limited size of the buffers, the collected data is regularly erased and replaced. A trigger signal is  
 786 needed for the TDC modules to send the useful data to the DAQ computer via a V1718 CAEN USB  
 787 communication module.

788 In the case of performance test, the trigger signal used for data acquisition is generated by the  
 789 coincidence of three scintillators. A first one is placed upstream outside of the bunker, a second one  
 790 is placed downstream outside of the bunker, while a third one is placed in front of the trolley, close by  
 791 the chambers. Every time a trigger is sent to the TDCs, i.e. every time a muon is detected, knowing  
 792 the time delay in between the trigger and the RPC signals, signals located in the right time window  
 793 are extracted from the buffers and saved for later analysis. Signals are taken in a time window of  
 794 400 ns centered on the muon peak (here we could show a time spectrum). On the other hand, in the  
 795 case of background rate measurement, the trigger signal needs to be "random" not to measure muons  
 796 but to look at gamma background. A trigger pulse is continuously generated at a rate of 300 Hz using  
 797 a dual timer. To integrate an as great as possible time, all signals contained within a time window of  
 798 10us prior to the random trigger signal are extracted form the buffers and saved for further analysis  
 799 (here another time spectrum to illustrate could be useful, maybe even place both spectrum together  
 800 as a single Figure).

801 The signals sent to the TDCs correspond to hit collections in the RPCs. When a particle hits  
 802 a RPC, it induce a signal in the pickup strips of the RPC readout. If this signal is higher than the  
 803 detection threshold, a LVDS signal is sent to the TDCs. The data is then organised into 4 branches  
 804 keeping track of the event number, the hit multiplicity for the whole setup, and the time and channel  
 805 profile of the hits in the TDCs.

### 806 5.3.2 RPC current, environmental and operation parameter monitoring

807 In order to take into account the variation of pressure and temperature between different data taking  
 808 periods the applied voltage is corrected following the relationship :

$$809 \text{HV}_{\text{eff}} = \text{HV}_{\text{app}} \times \left( 0.2 + 0.8 \cdot \frac{P_0}{P} \times \frac{T}{T_0} \right) \quad (5.10)$$

809 where  $T_0$  (=293 K) and  $P_0$  (=990 mbar) are the reference values.

810 **5.3.3 Measurement procedure**

- 811 Insert a short description of the online tools (DAQ, DCS, DQM).  
812 Insert a short description of the offline tools : tracking and efficiency algorithm.  
813 Identify long term aging effects we are monitoring the rates per strip.

814 **5.3.4 Longevity studies results**



# 6

815

816

## Investigation on high rate RPCs

817 **6.1 Rate limitations and ageing of RPCs**

818 **6.1.1 Low resistivity electrodes**

819 **6.1.2 Low noise front-end electronics**

820 **6.2 Construction of prototypes**

821 **6.3 Results and discussions**



# 7

822

823

## Conclusions and outlooks

<sup>824</sup> **7.1 Conclusions**

<sup>825</sup> **7.2 Outlooks**



## References

- [1] CERN. Geneva. LHC Experiments Committee. *The CMS muon project : Technical Design Report*. Tech. rep. CERN-LHCC-97-032. CMS Collaboration, 1997.
- [2] CERN. Geneva. LHC Experiments Committee. *Technical Proposal for the Phase-II Upgrade of the CMS Detector*. Tech. rep. CERN-LHCC-2015-010. CMS Collaboration, 2015.
- [3] CERN. Geneva. LHC Experiments Committee. *CMS, the Compact Muon Solenoid : technical proposal*. Tech. rep. CERN-LHCC-94-38. CMS Collaboration, 1994.
- [4] M. Abbrescia et al. “Study of long-term performance of CMS RPC under irradiation at the CERN GIF”. In: *NIMA* 533 (2004), pp. 102–106.
- [5] H.C. Kim et al. “Quantitative aging study with intense irradiation tests for the CMS forward RPCs”. In: *NIMA* 602 (2009), pp. 771–774.
- [6] S. Agosteo et al. “A facility for the test of large-area muon chambers at high rates”. In: *NIMA* 452 (2000), pp. 94–104.
- [7] PoS, ed. *CERN GIF ++ : A new irradiation facility to test large-area particle detectors for the high-luminosity LHC program*. Vol. TIPP2014. 2014, pp. 102–109.
- [8] M. Abbrescia et al. “Cosmic ray tests of double-gap resistive plate chambers for the CMS experiment”. In: *NIMA* 550 (2005), pp. 116–126.
- [9] A. Fagot. *GIF++ DAQ v4.0*. 2017. URL: [https://github.com/afagot/GIF\\_DAQ](https://github.com/afagot/GIF_DAQ).
- [10] CAEN. *Mod. V1190-VX1190 A/B, 128/64 Ch Multihit TDC*. 14th ed. 2016.
- [11] CAEN. *Mod. V1718 VME USB Bridge*. 9th ed. 2009.
- [12] W-Ie-Ne-R. *VME 6021-23 VXI*. 5th ed. 2016.
- [13] Wikipedia. *INI file*. 2017. URL: [https://en.wikipedia.org/wiki/INI\\_file](https://en.wikipedia.org/wiki/INI_file).
- [14] S. Carrillo A. Fagot. *GIF++ Offline Analysis v6*. 2017. URL: [https://github.com/afagot/GIF\\_OfflineAnalysis](https://github.com/afagot/GIF_OfflineAnalysis).



# A

850

851

## A data acquisition software for CAEN VME TDCs

852

853 Certifying detectors in the perspective of HL-LHC required to develop tools for the GIF++ experiment.  
854 Among them was the C++ Data Acquisition (DAQ) software that allows to make the com-  
855 munications in between a computer and TDC modules in order to retrieve the RPC data [9]. In this  
856 appendix, details about this software, as of how the software was written, how it functions and how  
857 it can be exported to another similar setup, will be given.

### 858 A.1 GIF++ DAQ file tree

859 GIF++ DAQ source code is fully available on github at [https://github.com/afagot/GIF\\_](https://github.com/afagot/GIF_DAQ)  
860 DAQ. The software requires 3 non-optional dependencies:

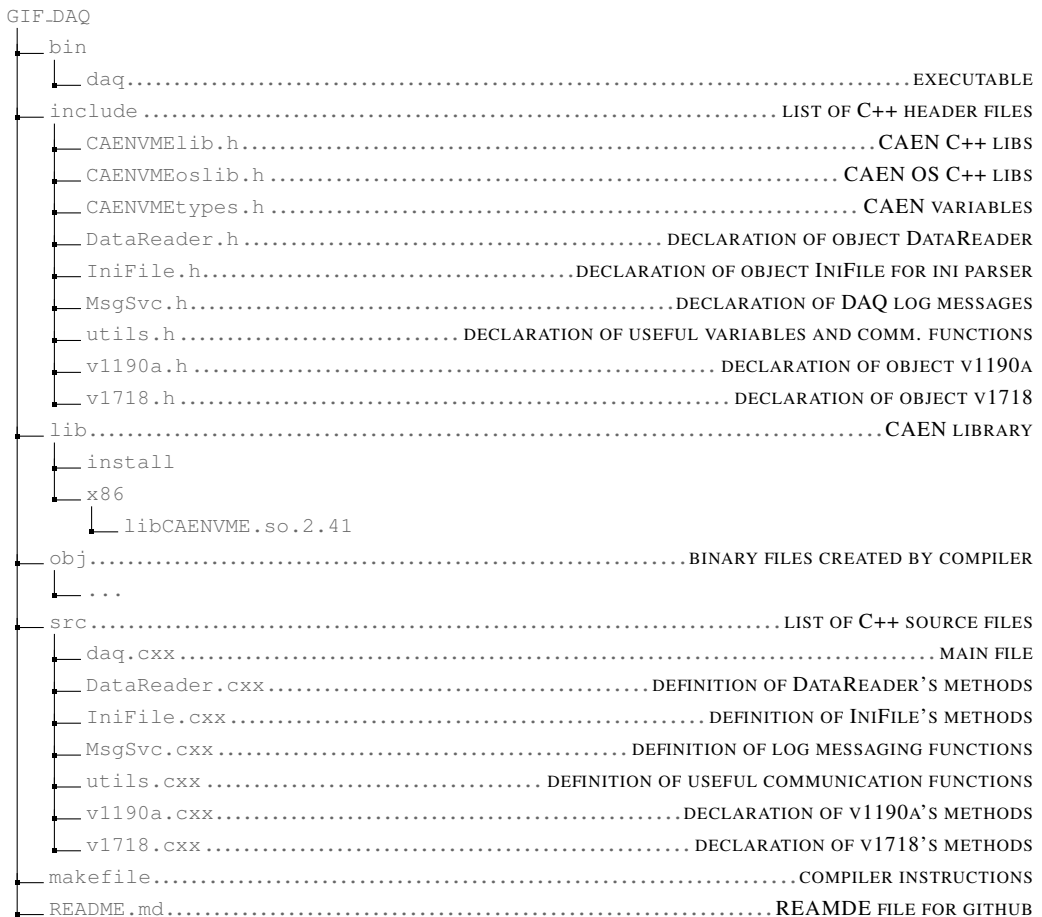
- 861 • CAEN USB Driver, to mount the VME hardware,  
862 • CAEN VME Library, to communicate with the VME hardware, and  
863 • ROOT, to organize the collected data into a TTree.

864 The CAEN VME library will not be packaged by distributions and will need to be installed man-  
865 ually. To compile the GIF++ DAQ project via a terminal, from the DAQ folder use the command:

866  
867 make

868 The source code tree is provided below along with comments to give an overview of the files' con-  
869 tent. The different objects created for this project (`v1718`, `v1190a`, `IniFile` & `DataReader`) will be  
870 described in details in the following sections.

871



## 872 A.2 Usage of the DAQ

873 GIF++ DAQ, as used in GIF++, is not a standalone software. Indeed, the system being more complex,  
 874 the DAQ only is a sub-layer of the software architecture developed to control and monitor  
 875 the RPCs that are placed into the bunker for performance study in an irradiated environment. The top  
 876 layer of GIF++ is a Web Detector Control System (webDCS) application. The DAQ is only called  
 877 by the webDCS when data needs to be acquired. The webDCS operates the DAQ through command  
 878 line. To start the DAQ, the webDCS calls:

879

880   bin/daq /path/to/the/log/file/in/the/output/data/folder

881 where /path/to/the/log/file/in/the/output/data/folder is the only argument required. This  
 882 log file is important for the webDCS as this file contains all the content of the communication of the  
 883 webDCS and the different systems monitored by the webDCS. Its content is constantly displayed  
 884 during data taking for the users to be able to follow the operations. The communication messages  
 885 are normally sent to the webDCS log file via the functions declared in file MsgSvc.h, typically  
 886 MSG\_INFO(string message).

887

### 888 A.3 Description of the readout setup

889 The CMS RPC setup at GIF++ counts 5 V1190A Time-to-Digital Converter (TDC) manufactured  
 890 by CAEN [10]. V1190A are VME units accepting 128 independent Multi-Hit/Multi-Event TDC  
 891 channels whose signals are treated by 4 100 ps high performance TDC chips developed by CERN  
 892 / ECP-MIC Division. The communication between the computer and the TDCs to transfer data is  
 893 done via a V1718 VME master module also manufactured by CAEN and operated from a USB  
 894 port [11]. These VME modules are all hosted into a 6U VME 6021 powered crate manufactured by  
 895 W-Ie-Ne-R than can accommodate up to 21 VME bus cards [12]. These 3 components of the DAQ  
 896 setup are shown in Figure A.1.

897

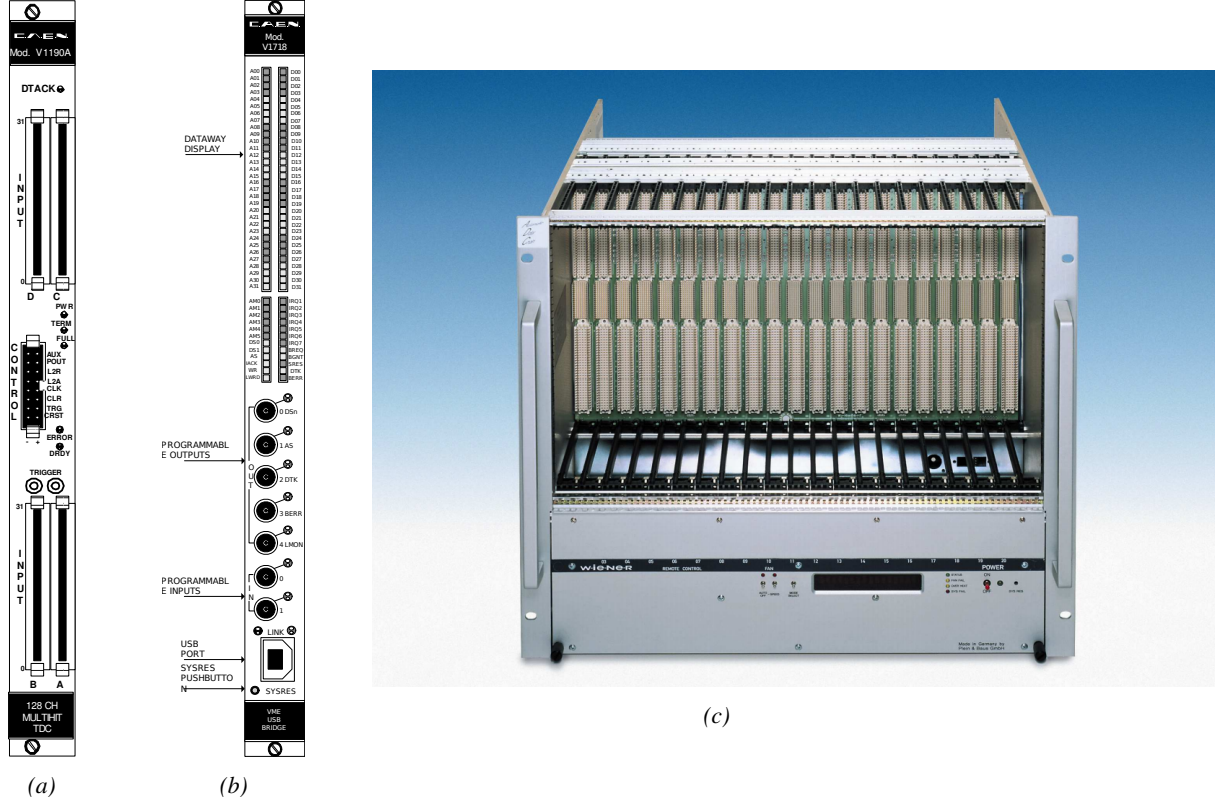


Figure A.1: (A.1a) View of the front panel of a V1190A TDC module [10]. (A.1b) View of the front panel of a V1718 Bridge module [11]. (A.1c) View of the front panel of a 6U 6021 VME crate [12].

898

### A.4 Data read-out

899 To efficiently perform a data readout algorithm, C++ objects to handle the VME modules (TDCs  
 900 and VME bridge) have been created along with objects to store data and read the configuration file

901 that comes as an input of the DAQ software.

902

### 903 A.4.1 V1190A TDCs

904 The DAQ used at GIF takes profit of the *Trigger Matching Mode* offered by V1190A modules.  
 905 This setting is enabled through the method `v1190a::SetTrigMatching (int ntdcs)` where `ntdcs`  
 906 is the total number of TDCs in the setup this setting needs to be enabled for (Source Code A.1). A  
 907 trigger matching is performed in between a trigger time tag, a trigger signal sent into the TRIGGER  
 908 input of the TDC visible on Figure A.1a, and the channel time measurements, signals recorded from  
 909 the detectors under test in our case. Control over this data acquisition mode, explained through  
 910 Figure A.2, is offered via 4 programmable parameters:

- 911 • **match window:** the matching between a trigger and a hit is done within a programmable time  
 912 window. This is set via the method

```
913     void v1190a::SetTrigWindowWidth(UINT windowWidth, int ntdcs)
```

- 914 • **window offset:** temporal distance between the trigger tag and the start of the trigger matching  
 915 window. This is set via the method

```
916     void v1190a::SetTrigWindowWidth(UINT windowWidth, int ntdcs)
```

- 917 • **extra search margin:** an extended time window is used to ensure that all matching hits are  
 918 found. This is set via the method

```
919     void v1190a::SetTrigSearchMargin(UINT searchMargin, int ntdcs)
```

- 920 • **reject margin:** older hits are automatically rejected to prevent buffer overflows and to speed  
 921 up the search time. This is set via the method

```
922     void v1190a::SetTrigRejectionMargin(UINT rejectMargin, int ntdcs)
```

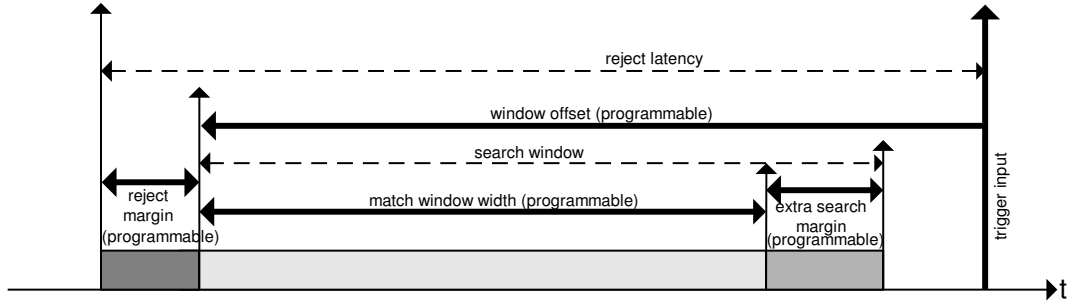


Figure A.2: Module V1190A Trigger Matching Mode timing diagram [10].

923 Each of these 4 parameters are given in number of clocks, 1 clock being 25 ns long. It is easy to  
 924 understand at this level that there are 3 possible functioning settings:

- 925 • **1:** the match window is entirely contained after the trigger signal,

- 926 • **2:** the match window overlaps the trigger signal, or

- 927 • **3:** the match window is entirely contained before the trigger signal as displayed on Figure A.2.

928 In both the first and second cases, the sum of the window width and of the offset can be set to  
929 a maximum of 40 clocks, which corresponds to 1  $\mu$ s. Evidently, the offset can be negative, allowing  
930 for a longer match window, with the constraint of having the window ending at most 1  $\mu$ s after the  
931 trigger signal. In the third case, the maximum negative offset allowed is of 2048 clocks (12 bit) cor-  
932 responding to 51.2  $\mu$ s, the match window being strictly smaller than the offset. In the case of GIF++,  
933 the choice has been made to use this last setting by delaying the trigger signal. During the studies  
934 performed in GIF++, both the efficiency of the RPCs, probed using a muon beam, and the noise or  
935 gamma background rate are monitored. The extra search and reject margins are left unused.  
936 To probe the efficiency of RPC detectors, the trigger time tag is provided by the coïncidence of  
937 scintillators when a bunch of muons passes through GIF++ area is used to trigger the data acquisi-  
938 tion. For this measurement, it is useful to reduce the match window width only to contain the muon  
939 information. Indeed, the delay in between a trigger signal and the detection of the corresponding  
940 muon in the RPC being very contant (typically a few tens of ns due to jitter and cable length), the  
941 muon signals are very localised in time. Thus, due to a delay of approximalety 325 ns in between  
942 the muons and the trigger, the settings where chosen to have a window width of 24 clocks (600 ns)  
943 centered on the muon peak thanks to a negative offset of 29 clocks (725 ns).  
944 On the otherhand, monitoring the rates don't require for the DAQ to look at a specific time window.  
945 It is important to integrate enough time to have a robust measurement of the rate as the number of  
946 hits per time unit. The triggerring signal is provided by a pulse generator at a frequency of 300 Hz  
947 to ensure that the data taking occurs in a random way, with respect to beam physics, to probe only  
948 the irradiation spectrum on the detectors. The match window is set to 400 clocks (10  $\mu$ s) and the  
949 negative offset to 401 clocks as it needs to exceed the value of the match window.

```
950 class v1190a
{
    private :
        long             Handle;
        vector<Data32>   Address;
        CVDataWidth       DataWidth;
        CVAddressModifier AddressModifier;

    public:

        v1190a(long handle, IniFile *inifile, int ntdcs);
        ~v1190a();
        Data16 write_op_reg(Data32 address, int code, string error);
        Data16 read_op_reg(Data32 address, string error);
        void Reset(int ntdcs);
        void Clear(int ntdcs);
        void TestWR(Data16 value,int ntdcs);
        void CheckTDCStatus(int ntdcs);
        void CheckCommunication(int ntdcs);
        void SetTDCTestMode(Data16 mode,int ntdcs);
        void SetTrigMatching(int ntdcs);
        void SetTrigTimeSubstraction(Data16 mode,int ntdcs);
        void SetTrigWindowWidth(Uint windowHeight,int ntdcs);
        void SetTrigWindowOffset(Uint windowOffset,int ntdcs);
        void SetTrigSearchMargin(Uint searchMargin,int ntdcs);
        void SetTrigRejectionMargin(Uint rejectMargin,int ntdcs);
        void GetTrigConfiguration(int ntdcs);
        void SetTrigConfiguration(IniFile *inifile,int ntdcs);
        void SetTDCDetectionMode(Data16 mode,int ntdcs);
        void SetTDCResolution(Data16 lsb,int ntdcs);
        void SetTDCDeadTime(Data16 time,int ntdcs);
        void SetTDCHeadTrailer(Data16 mode,int ntdcs);
        void SetTDCEventSize(Data16 size,int ntdcs);
        void SwitchChannels(IniFile *inifile,int ntdcs);
        void SetIRQ(Data32 level, Data32 count,int ntdcs);
        void SetBlockTransferMode(Data16 mode,int ntdcs);
        void Set(IniFile *inifile,int ntdcs);
        void CheckStatus(CVErrorCodes status) const;
        int ReadBlockD32(Uint tdc, const Data16 address,
                         Data32 *data, const Uint words, bool ignore_berr)
        Uint Read(RAWData *DataList,int ntdcs);
};


```

952 *Source Code A.1: Description of C++ object v1190a.*

The v1190a object, defined in the DAQ software as in Source Code A.1, offers the possibility to concatenate all TDCs in the readout setup into a single object containing a list of hardware addresses (addresses to access the TDCs' buffer through the VME crate) and each constructor and method acts on the list of TDCs.

958 A.4.2 DataReader

Enabled thanks to `v1190a::SetBlockTransferMode(Data16 mode, int ntdcs)`, the data transfer is done via Block Transfer (BLT). Using BLT allows to tranfer a fixed number of events called a *block*. This is used together with an Almost Full Level (AFL) of the TDCs' output buffers, defined

962 through `v1190a::SetIRQ(Data32 level, Data32 count, int ntdcs)`. This AFL gives the maximum amount of 32735 words (16 bits, corresponding to the depth of a TDC output buffer) that can  
 963 written in a buffer before an Interrupt Request (IRQ) is generated and seen by the VME Bridge,  
 964 stopping the data acquisition to transfer the content of each TDC buffers before resuming. For each  
 965 trigger, 6 words or more are written into the TDC buffer:

- 967     • a **global header** providing information of the event number since the beginning of the data  
       acquisition,
- 969     • a **TDC header**,
- 970     • the **TDC data** (*if any*), 1 for each hit recorded during the event, providing the channel and the  
       time stamp associated to the hit,
- 972     • a **TDC error** providing error flags,
- 973     • a **TDC trailer**,
- 974     • a **global trigger time tag** that provides the absolute trigger time relatively to the last reset,  
       and
- 976     • a **global trailer** providing the total word count in the event.

977     As previously described in Section 4.4.3, CMS RPC FEEs provide us with 100 ns long LVDS  
 978 output signals that are injected into the TDCs' input. Any avalanche signal that gives a signal above  
 979 the FEEs threshold is thus recorded by the TDCs as a hit within the match window. Each hit is  
 980 assigned to a specific TDC channel with a time stamp, with a precision of 100 ps. The reference  
 981 time,  $t_0 = 0$ , is provided by the beginning of the match window. Thus for each trigger, coming from  
 982 a scintillator coïncidence or the pulse generator, a list of hits is stored into the TDCs' buffers and  
 983 will then be transferred into a ROOT Tree.

984  
 985     When the BLT is used, it is easy to understand that the maximum number of words that have  
 986 been set as ALF will not be a finite number of events or, at least, the number of events that would  
 987 be recorded into the TDC buffers will not be a multiple of the block size. In the last BLT cycle to  
 988 transfer data, the number of events to transfer will most probably be lower than the block size. In that  
 989 case, the TDC can add fillers at the end of the block but this option requires to send more data to the  
 990 computer and is thus a little slower. Another solution is to finish the transfer after the last event by  
 991 sending a bus error that states that the BLT reached the last event in the pile. This method has been  
 992 chosen in GIF++.

993  
 994     Due to irradiation, an event in GIF++ can count up to 300 words per TDC. A limit of 4096 words  
 995 (12 bits) has been set to generate IRQ which represent from 14 to almost 700 events depending on  
 996 the average of hits collected per event. Then the block size has been set to 100 events with enabled  
 997 bus errors. When an AFL is reached for one of the TDCs, the VME bridge stops the acquisition by  
 998 sending a BUSY signal.

999

1000       The data is then transferred one TDC at a time into a structure called `RAWData` (Source Code A.2).

```
1001
1002     struct RAWData{
1003         vector<int>           *EventList;
1004         vector<int>           *NHitsList;
1005         vector<int>           *QFlagList;
1006         vector<vector<int>>   *Channellist;
1007         vector<vector<float>>  *TimeStampList;
1008     };
```

1003                     *Source Code A.2: Description of data holding C++ structure `RAWData`.*

1004       In order to organize the data transfer and the data storage, an object called `DataReader` was
1005       created (Source Code A.3). On one hand, it has `v1718` and `v1190a` objects as private members for
1006       communication purposes, such as VME modules settings via the configuration file `*iniFile` or data
1007       read-out through `v1190a::Read()` and on the other hand, it contains the structure `RAWData` that allows
1008       to organise the data in vectors reproducing the tree structure of a ROOT file.

```
1009
1010    class DataReader
1011    {
1012        private:
1013            bool      StopFlag;
1014            IniFile *iniFile;
1015            Data32   MaxTriggers;
1016            v1718   *VME;
1017            int       nTDCs;
1018            v1190a  *TDCs;
1019            RAWData TDCData;
1020
1021        public:
1022            DataReader();
1023            virtual ~DataReader();
1024            void      SetIniFile(string inifilename);
1025            void      SetMaxTriggers();
1026            Data32   GetMaxTriggers();
1027            void      SetVME();
1028            void      SetTDC();
1029            int       GetQFlag(Uint it);
1030            void      Init(string inifilename);
1031            void      FlushBuffer();
1032            void      Update();
1033            string   GetFileName();
1034            void      WriteRunRegistry(string filename);
1035            void      Run();
1036    };
```

1011                     *Source Code A.3: Description of C++ object `DataReader`.*

1012       Each event is transferred from `TDCData` and saved into branches of a ROOT `TTree` as 3 integers
1013       that represent the event ID (`EventCount`), the number of hits read from the TDCs (`nHits`), and the
1014       quality flag that provides information for any problem in the data transfer (`qflag`), and 2 lists of
1015       `nHits` elements containing the fired TDC channels (`TDCCh`) and their respective time stamps (`TDCTS`),
1016       as presented in Source Code A.4. The ROOT file file is named using information contained into
1017       the configuration file, presented in section A.5.2. The needed information is extracted using method
1018       `DataReader::GetFileName()` and allow to build the output filename format `ScanXXXXXX_HVX_DAQ.root`

1019 where ScanXXXXXX is a 6 digit number representing the scan number into GIFT++ database and HVX  
 1020 the HV step within the scan that can be more than a single digit. An example of ROOT data file is  
 1021 provided with Figure A.3.

```
1022
RAWData TDCData;
TFile *outputFile = new TFile(outputFileName.c_str(),"recreate");
TTree *RAWDataTree = new TTree("RAWData","RAWData");

int EventCount = -9;
int nHits = -8;
int qflag = -7;
vector<int> TDCCh;
vector<float> TDCTS;

RAWDataTree->Branch("EventNumber",&EventCount, "EventNumber/I");
RAWDataTree->Branch("number_of_hits",&nHits,"number_of_hits/I");
RAWDataTree->Branch("Quality_flag",&qflag,"Quality_flag/I");
RAWDataTree->Branch("TDC_channel",&TDCCh);
RAWDataTree->Branch("TDC_TimeStamp",&TDCTS);

1023
//...
//Here read the TDC data using v1190a::Read() and place it into
//TDCData for as long as you didn't collect the requested amount
//of data.
//...

for(Uint i=0; i<TDCData.EventList->size(); i++){
    EventCount = TDCData.EventList->at(i);
    nHits = TDCData.NHitsList->at(i);
    qflag = TDCData.QFlagList->at(i);
    TDCCh = TDCData.ChannelList->at(i);
    TDCTS = TDCData.TimeStampList->at(i);
    RAWDataTree->Fill();
}
```

1024 *Source Code A.4: Highlight of the data transfer and organisation within DataReader::Run() after the data has been collected into TDCData.*

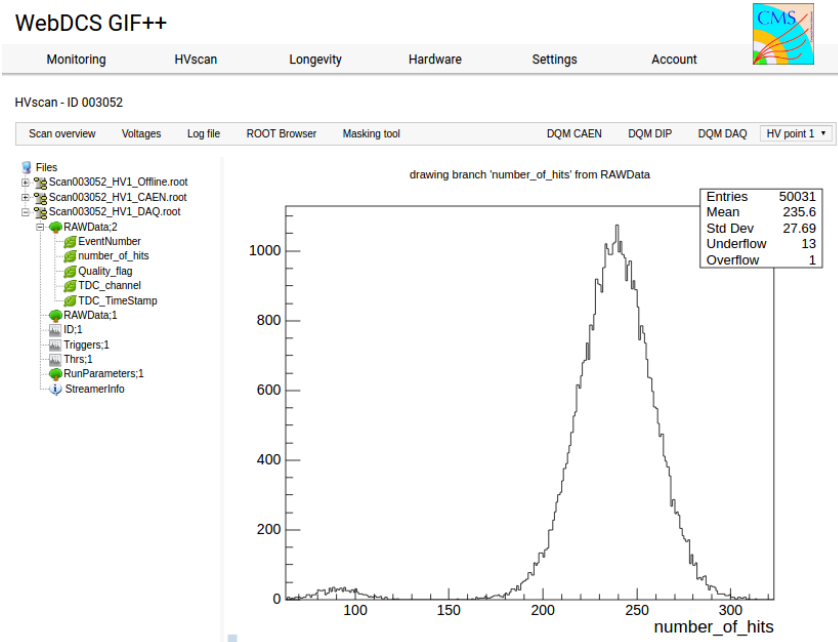


*Figure A.3: Structure of the ROOT output file generated by the DAQ. The 5 branches (EventNumber, number\_of\_hits, Quality\_flag, TDC\_channel and TDC\_TimeStamp) are visible on the left panel of the ROOT browser. On the right panel is visible the histogram corresponding to the variable nHits. In this specific example, there were approximately 50k events recorded to measure the gamma irradiation rate on the detectors. Each event is stored as a single entry in the TTree.*

#### 1025 A.4.3 Data quality flag

1026 Among the parameters that are recorded for each event, the quality flag, defined in Source Code A.5,  
 1027 is determined on the fly by checking the data recorded by every single TDC. From method `v1190a::Read()`,  
 1028 it can be understood that the content of each TDC buffer is readout one TDC at a time. Entries are  
 1029 created in the data list for the first TDC and then, when the second buffer is readout, events corre-  
 1030 sponding to entries that have already been created to store data for the previous TDC are added to  
 1031 the existing list element. On the contrary, when an event entry has not been yet created in the data  
 1032 list, a new entry is created.

```
1033 typedef enum _QualityFlag {
 1034     GOOD      = 1,
     CORRUPTED = 0
 } QualityFlag;
```

1035 *Source Code A.5: Definition of the quality flag `enum`.*

1036 It is possible that each TDC buffer contains a different number of events. In cases where the first  
 1037 element in the buffer list is an event for corresponds to a new entry, the difference in between the  
 1038 entry from the buffer and the last entry in the data list is recorded and checked. If it is greater than 1,  
 1039 what should never be the case, the quality flag is set to CORRUPTED for this TDC and an empty entry  
 1040 is created in the place of the missing ones.

1041 At the end of each BLT cycle, the ID of the last entry stored for each TDC buffer is not recorded.  
 1042 When starting the next cycle, if the first entry in the pile corresponds to an event already existing  
 1043 in the list, the readout will start from this list element and will not be able to check the difference  
 1044 in between this entry's ID and the one of the last entry that was recorded for this TDC buffer in  
 1045 the previous cycle. In the case events were missing, the flag stays at its initial value of 0, which is  
 1046 similar to CORRUPTED and it is assumed that then this TDC will not contribute to number\_of\_hits,  
 1047 TDC\_channel or TDC\_TimeStamp.

1048 Finally, since there will be 1 RAWData entry per TDC for each event (meaning nTDCs entries,  
 1049 referring to DataReader private attribute), the individual flags of each TDC will be added together.  
 1050 The final format is an integer composed nTDCs digits where each digit is the flag of a specific TDC.  
 1051 This is constructed using powers of 10 like follows:

1052 TDC 0: QFlag =  $10^0 \times \text{QualityFlag}$

1053 TDC 1: QFlag =  $10^1 \times \text{QualityFlag}$

1054 ...

1055 TDC N: QFlag =  $10^N \times \text{QualityFlag}$

1056 and the final flag to be with N digits:

1057 QFlag = n....3210

1058 each digit being 1 or 0. Below is given an example with a 4 TDCs setup.

1059 If all TDCs were good : QFlag = 1111,

1060 but if TDC 2 was corrupted : QFlag = 1011.

1061 When data taking is over and the data contained in the dynamical RAWData structure is transferred  
 1062 to the ROOT file, all the 0s are changed into 2s by calling the method DataReader::GetQFlag().  
 1063 This will help translating the flag without knowing the number of TDCs beforehand. Indeed, a flag  
 1064 111 could be due to a 3 TDC setup with 3 good individual TDC flags or to a more than 3 TDC setup  
 1065 with TDCs those ID is greater than 2 being CORRUPTED, thus giving a 0.

1066 The quality flag has been introduced quite late, in October 2017 only, to the list of GIFT++ DAQ  
 1067 parameters to be recorded into the output ROOT file. Before this addition, the missing data, corrupting  
 1068 the quality for the offline analysis, was contributing to artificially fill data with lower multiplicity  
 1069 in TBranch number\_of\_hits and thus, the multiplicity 0 bin of reconstructed events, as can be re-  
 1070 spectively seen in Figure A.4 and A.5.

1071

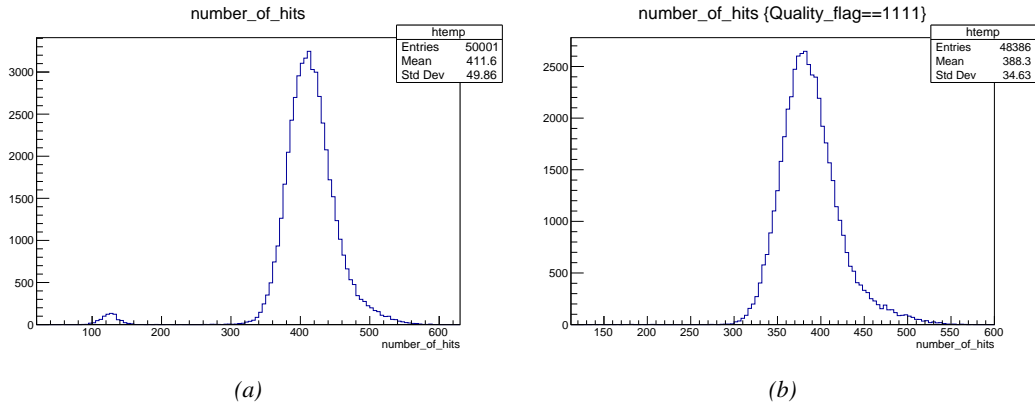


*Figure A.4: The effect of the quality flag is explained by presenting the content of TBranch `number_of_hits` of a data file without `Quality_flag` in Figure A.4a and the content of the same TBranch for data corresponding to a `Quality_flag` where all TDCs were labelled as `GOOD` in Figure A.4b taken with similar conditions. It can be noted that the number of entries in Figure A.4b is slightly lower than in Figure A.4a due to the excluded events.*

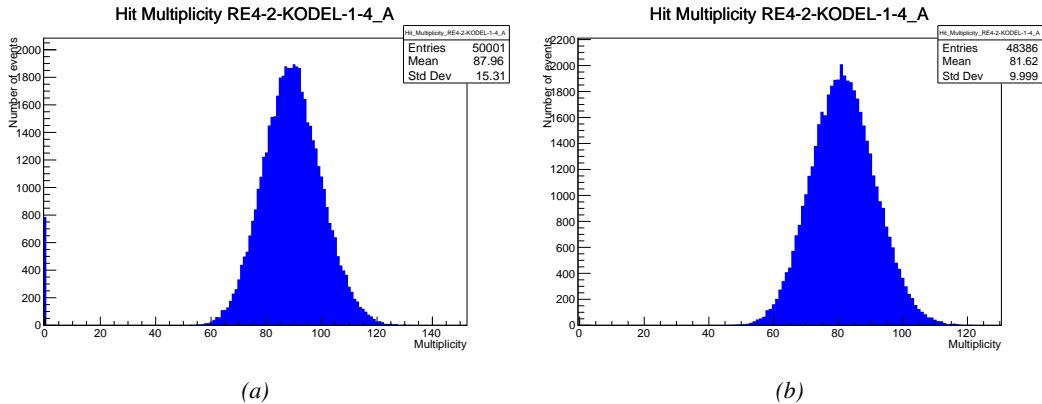


*Figure A.5: Using the same data as previously showed in Figure A.4, the effect of the quality flag is explained by presenting the reconstructed hit multiplicity of a data file without `Quality_flag` in Figure A.5a and the reconstructed content of the same RPC partition for data corresponding to a `Quality_flag` where all TDCs were labelled as `GOOD` in Figure A.5b taken with similar conditions. The artificial high content of bin 0 is completely suppressed.*

## 1072 A.5 Communications

1073 To ensure data readout and dialog in between the machine and the TDCs or in between the webDCS  
 1074 and the DAQ, different communication solutions were used. First of all, it is important to have a  
 1075 module to allow the communication in between the TDCs and the computer from which the DAQ  
 1076 operates. When this communication is effective, shifters using the webDCS to control data taking  
 1077 can thus send instructions to the DAQ.

1078

### 1079 A.5.1 V1718 USB Bridge

1080 In the previous section, the data transfer has been discussed. The importance of the `v1718` object  
 1081 (Source Code A.6), used as private member of `DataReader`, was not explicated. VME master  
 1082 modules are used for communication purposes as they host the USB port that connects the pow-  
 1083 ered crate buffer to the computer where the DAQ is installed. From the source code point of view,  
 1084 this object is used to control the communication status, by reading the returned error codes with  
 1085 `v1718::CheckStatus()`, or to check for IRQs coming from the TDCs through `v1718::CheckIRQ()`.  
 1086 Finally, to ensure that triggers are blocked at the hardware level, a NIM pulse is sent out of one of the  
 1087 5 programmable outputs (`v1718::SendBUSY()`) to the VETO of the coincidence module where the  
 1088 trigger signals originate from. As long as this signal is ON, no trigger can reach the TDCs anymore.

```
1089
1090 class v1718{
1091     private:
1092         int             Handle;
1093         Data32          Data;           // Data
1094         CVIRQLevels    Level;         // Interrupt level
1095         CVAddressModifier AM;         // Addressing Mode
1096         CVDataWidth     DataSize;      // Data Format
1097         Data32          BaseAddress;   // Base Address
1098
1099     public:
1100         v1718(IniFile *inifile);
1101         ~v1718();
1102         long            GetHandle(void) const;
1103         int             SetData(Data16 data);
1104         Data16          GetData(void);
1105         int             GetLevel(CVIRQLevels level);
1106         CVIRQLevels    GetLevel(void);
1107         int             SetAM(CVAddressModifier am);
1108         CVAddressModifier GetAM(void);
1109         int             SetDatasize(CVDataWidth datasize);
1110         CVDataWidth     GetDataSize(void);
1111         int             SetBaseAddress(Data16 baseaddress);
1112         Data16          GetBaseAddress(void);
1113         void            CheckStatus(CVErrorCodes status) const;
1114         bool            CheckIRQ();
1115         void            SetPulsers();
1116         void            SendBUSY(BusyLevel level);
1117     };

```

1091 *Source Code A.6: Description of C++ object v1718.*

### 1092 A.5.2 Configuration file

1093 The DAQ software takes as input a configuration file written using INI standard [13]. This file is  
 1094 partly filled with the information provided by the shifters when starting data acquisition using the  
 1095 webDCS, as shown by Figure A.6. This information is written in section [`General`] and will later  
 1096 be stored in the ROOT file that contains the DAQ data as can be seen from Figure A.3. Indeed,  
 1097 another `TTree` called `RunParameters` as well as the 2 histograms `ID`, containing the scan number,  
 1098 start and stop time stamps, and `Triggers`, containing the number of triggers requested by the shifter,  
 1099 are available in the data files. Moreover, `ScanID` and `HV` are then used to construct the file name  
 1100 thanks to the method `DataReader::GetFileName()`.

**WebDCS GIF++**

---

Monitoring    HVscan    Longevity    Hardware    Settings    Account

DAQ High Voltage Scan

Type scan: Rate Scan    Comments:

Source configuration: Source OFF    U 333    D 333    HV after scan: Turn off

Beam configuration: Beam OFF

Waiting time: 1 (min)

Trigger mode:  External  Internal  Random

Minimal measure time: 10 (min)

Chamber	RE2-2-NPD-BARC-8	RE2-2-CERN-105	RE2-2-NPD-BARC-9	RE4-2-CERN-105	RE4-2-KODEL-1-4	Max triggers
HV <sub>eff</sub> 1	8600	8500	8600	8500	6500	<input type="text"/>
HV <sub>eff</sub> 2	8700	8600	8700	8600	6600	<input type="text"/>
HV <sub>eff</sub> 3	8800	8700	8800	8700	6700	<input type="text"/>
HV <sub>eff</sub> 4	8900	8800	8900	8800	6800	<input type="text"/>
HV <sub>eff</sub> 5	9000	8900	9000	8900	6900	<input type="text"/>
HV <sub>eff</sub> 6	9100	9000	9100	9000	7000	<input type="text"/>
HV <sub>eff</sub> 7	9200	9100	9200	9100	7100	<input type="text"/>
HV <sub>eff</sub> 8	9300	9200	9300	9200	7200	<input type="text"/>
HV <sub>eff</sub> 9	9400	9300	9400	9300	7300	<input type="text"/>
HV <sub>eff</sub> 10	9500	9400	9500	9400	7400	<input type="text"/>

**Start HV scan**

*Figure A.6: WebDCS DAQ scan page. On this page, shifters need to choose the type of scan (Rate, Efficiency or Noise Reference scan), the gamma source configuration at the moment of data taking, the beam configuration, and the trigger mode. These information will be stored in the DAQ ROOT output. Are also given the minimal measurement time and waiting time after ramping up of the detectors is over before starting the data acquisition. Then, the list of HV points to scan and the number of triggers for each run of the scan are given in the table underneath.*

1101     The rest of the information is written beforehand in the configuration file template, as explicated  
 1102     in Source Code A.7, and contains the hardware addresses to the different VME modules in the  
 1103     setup as well as settings for the TDCs. As the TDC settings available in the configuration file are not  
 1104     supposed to be modified, an improvement would be to remove them from the configuration file and  
 1105     to hardcode them inside of the DAQ code itself or to place them into a different INI file that would  
 1106     host only the TDC settings to lower the probability for a bad manipulation of the configuration file  
 1107     that can be modified from one of webDCS' menus.

```

1108
[General]
Tdcs=4
ScanID=$scanid
HV=$HV
RunType=$runtype
MaxTriggers=$maxtriggers
Beam=$beam
[VMEInterface]
Type=V1718
BaseAddress=0xFF0000
Name=VmeInterface
[TDC0]
Type=V1190A
BaseAddress=0x00000000
Name=Tdc0
StatusA00-15=1
StatusA16-31=1
StatusB00-15=1
StatusB16-31=1
StatusC00-15=1
StatusC16-31=1
StatusD00-15=1
StatusD16-31=1
[TDC1]
Type=V1190A
BaseAddress=0x11110000
Name=Tdc1
StatusA00-15=1
StatusA16-31=1
StatusB00-15=1
StatusB16-31=1
StatusC00-15=1
StatusC16-31=1
StatusD00-15=1
StatusD16-31=1
1109
[TDC2]
Type=V1190A
BaseAddress=0x22220000
Name=Tdc2
StatusA00-15=1
StatusA16-31=1
StatusB00-15=1
StatusB16-31=1
StatusC00-15=1
StatusC16-31=1
StatusD00-15=1
StatusD16-31=1
[TDC3]
Type=V1190A
BaseAddress=0x44440000
Name=Tdc3
StatusA00-15=1
StatusA16-31=1
StatusB00-15=1
StatusB16-31=1
StatusC00-15=1
StatusC16-31=1
StatusD00-15=1
StatusD16-31=1
[TDCSettings]
TriggerExtraSearchMargin=0
TriggerRejectMargin=0
TriggerTimeSubstraction=0b1
TdcDetectionMode=0b01
TdcResolution=0b10
TdcDeadTime=0b00
TdcHeadTrailer=0b1
TdcEventSize=0b1001
TdcTestMode=0b0
BLTMode=1

```

*Source Code A.7: INI configuration file template for 4 TDCs. In section [General], the number of TDCs is explicitated and information about the ongoing run is given. Then, there are sections for each and every VME modules. There buffer addresses are given and for the TDCs, the list of channels to enable is given. Finally, in section [TDCSettings], a part of the TDC settings are given.*

1111     In order to retrieve the information of the configuration file, the object `IniFile` has been developed  
 1112     to provide an INI parser, presented in Source Code A.8. It contains private methods returning a  
 1113     boolean to check the type of line written in the file, whether a comment, a group header or a key line  
 1114     (`IniFile::CheckIfComment()`, `IniFile::CheckIfGroup()` and `IniFile::CheckIfToken()`). The  
 1115     key may sometimes be referred to as *token* in the source code. Moreover, the private element  
 1116     `FileData` is a map of `const string` to `string` that allows to store the data contained inside the  
 1117     configuration file via the public method `IniFile::GetFileData()` following the formatting (see  
 1118     method `IniFile::Read()`):

```
1119     string group, token, value;
  // Get the field values for the 3 strings.
  // Then concatenate group and token together as a single string
  // with a dot separation.
  token = group + "." + token;
  FileData[token] = value;
```

1121     More methods have been written to translate the different keys into the right variable format  
 1122     when used by the DAQ. For example, to get a `float` value out of the configuration file data, knowing  
 1123     the group and the key needed, the method `IniFile::floatType()` can be used. It takes 3 arguments  
 1124     being the group name and key name (both `string`), and a default `float` value used as exception in  
 1125     the case the expected combination of group and key cannot be found in the configuration file. This  
 1126     default value is then used and the DAQ continues on working after sending an alert in the log file for  
 1127     further debugging.

```

1128 typedef map< const string, string > IniFileData;
1129
class IniFile{
    private:
        bool          CheckIfComment (string line);
        bool          CheckIfGroup(string line, string& group);
        bool          CheckIfToken(string line, string& key, string& value);
        string         FileName;
        IniFileData   FileData;
        int           Error;

    public:
        IniFile();
        IniFile(string filename);
        virtual      ~IniFile();

        // Basic file operations
        void          SetFileName(string filename);
        int           Read();
        int           Write();
        IniFileData   GetFileData();

        // Data readout methods
        Data32         addressType (string groupname, string keyname, Data32
→     defaultvalue);
        long          intType     (string groupname, string keyname, long
→     defaultvalue);
        long long    longType    (string groupname, string keyname, long long
→     defaultvalue );
        string         stringType  (string groupname, string keyname, string
→     defaultvalue );
        float         floatType   (string groupname, string keyname, float
→     defaultvalue );

        // Error methods
        string         GetErrorMsg();
};

1130

```

*Source Code A.8: Description of C++ object `IniFile` used as a parser for INI file format.*

### A.5.3 WebDCS/DAQ intercommunication

When shifters send instructions to the DAQ via the configuration file, it is the webDCS itself that gives the start command to the DAQ and then the 2 softwares use inter-process communication through file to synchronise themselves. This communication file is represented by the variable **const string \_\_runstatuspath**.

On one side, the webDCS sends commands or status that are readout by the DAQ:

- INIT, status sent when launching a scan and read via function `CtrlRunStatus(...)`,
- START, command to start data taking and read via function `CheckSTART()`,
- STOP, command to stop data taking at the end of the scan and read via function `CheckSTOP()`, and
- KILL, command to kill data taking sent by user and read via function `CheckKILL()`

and on the other, the DAQ sends status that are controled by the webDCS:

- 1143     ● `DAQ_RDY`, sent with `SendDAQReady()` to signify that the DAQ is ready to receive commands  
1144       from the webDCS,
- 1145     ● `RUNNING`, sent with `SendDAQRunning()` to signify that the DAQ is taking data,
- 1146     ● `DAQ_ERR`, sent with `SendDAQError()` to signify that the DAQ didn't receive the expected com-  
1147       mand from the webDCS or that the launch command didn't have the right number of argu-  
1148       ments,
- 1149     ● `RD_ERR`, sent when the DAQ wasn't able to read the communication file, and
- 1150     ● `WR_ERR`, sent when the DAQ wasn't able to write into the communication file.

#### 1151     **A.5.4 Example of inter-process communication cycle**

1152     Under normal conditions, the webDCS and the DAQ processes exchange commands and status via  
1153       the file hosted at the address `__runstatuspath`, as explained in subsection A.5.3. An example of  
1154       cycle is given in Table A.1. In this example, the steps 3 to 5 are repeated as long as the webDCS tells  
1155       the DAQ to take data. A data taking cycle is the equivalent as what is called a *Scan* in GIFT++ jargon,  
1156       referring to a set a runs with several HV steps. Each repetition of steps 3 to 5 is then equivalent to a  
1157       single *Run*.

1158

1159     At any moment during the data taking, for any reason, the shifter can decide that the data taking  
1160       needs to be stopped before it reached the end of the scheduled cycle. Thus at any moment on the  
1161       cycle, the content of the inter-process communication file will be changed to `KILL` and the DAQ will  
1162       shut down right away. The DAQ checks for `KILL` signals every 5s after the TDCs configuration is  
1163       over. So far, the function `CheckKILL()` has been used only inside of the data taking loop of method  
1164       `DataReader::Run()` and thus, if the shifter decides to KILL the data taking during the TDC con-  
1165       figuration phase or the HV ramping in between 2 HV steps, the DAQ will not be stopped smoothly  
1166       and a *force kill* command will be sent to stop the DAQ process that is still awake on the computer.  
1167       Improvements can be brought on this part of the software to make sure that the DAQ can safely  
1168       shutdown at any moment.

1169

### 1170     **A.6 Software export**

1171     In section A.2 was discussed the fact that the DAQ as written in its last version is not a standalone  
1172       software. It is possible to make it a standalone program that could be adapted to any VME setup  
1173       using V1190A and V1718 modules by creating a GUI for the software or by printing the log mes-  
1174       sages that are normally printed in the webDCS through the log file, directly into the terminal. This  
1175       method was used by the DAQ up to version 3.0 moment where the webDCS was completed. Also, it  
1176       is possible to check branches of DAQ v2.X to have example of communication through a terminal.

1177

1178     DAQ v2.X is nonetheless limited in it's possibilities and requires a lot of offline manual interven-  
1179       tions from the users. Indeed, there is no communication of the software with the detectors' power  
1180       supply system that would allow for a user a predefine a list of voltages to operate the detectors at

step	actions of webDCS	status of DAQ	<code>__runstatuspath</code>
1	launch DAQ ramp voltages ramping over wait for currents stabilization	readout of IniFile configuration of TDCs	INIT
2		configuration done send DAQ ready wait for START signal	DAQ_RDY
3	waiting time over send START		START
4	wait for run to end monitor DAQ run status	data taking ongoing check for KILL signal	RUNNING
5		run over send DAQ_RDY wait for next DCS signal	DAQ_RDY
6	ramp voltages ramping over wait for currents stabilization		DAQ_RDY
3	waiting time over send START		START
4	wait for run to end monitor DAQ run status	update IniFile information data taking ongoing check for KILL signal	RUNNING
5		run over send DAQ_RDY wait for next DCS signal	DAQ_RDY
7	send command STOP	DAQ shuts down	STOP

Table A.1: Inter-process communication cycles in between the webDCS and the DAQ through file string signals.

1181 and loop over to take data without any further manual intervention. In v2.X, the data is taken for a  
1182 single detector setting and at the end of each run, the softwares asks the user if he intends on taking  
1183 more runs. If so, the software invites the user to set the operating voltages accordingly to what is  
1184 necessary and to manual update the configuration file in consequence. This working mode can be a  
1185 very first approach before an evolution and has been successfully used by colleagues from different  
1186 collaborations.

1187

1188 For a more robust operation, it is recommended to develop a GUI or a web application to inter-  
1189 face the DAQ. Moreover, to limit the amount of manual interventions, and thus the probability to  
1190 make mistakes, it is also recommended to add an extra feature into the DAQ by installing the HV  
1191 Wrapper library provided by CAEN of which an example of use in a similar DAQ software devel-  
1192 opped by a master student of UGent, and called TinyDAQ, is provided on UGent's github. Then, this  
1193 HV Wrapper will help you communicating with and give instructions to a CAEN HV powered crate  
1194 and can be added into the DAQ at the same level where the communication with the user was made  
1195 in DAQ v2.X. In case you are using another kind of power system for your detectors, it is stringly  
1196 adviced to use HV modules or crates that can be remotely controled via a using C++ libraries.

1197

# B

1198

1199

## Details on the offline analysis package

1200 The data collected in GIF++ thanks to the DAQ described in Appendix A is difficult to interpret by  
1201 a human user that doesn't have a clear idea of the raw data architecture of the ROOT data files. In  
1202 order to render the data human readable, a C++ offline analysis tool was designed to provide users  
1203 with detector by detector histograms that give a clear overview of the parameters monitored during  
1204 the data acquisition [14]. In this appendix, details about this software in the context of GIF++, as of  
1205 how the software was written and how it functions will be given.

### 1206 B.1 GIF++ Offline Analysis file tree

1207 GIF++ Offline Analysis source code is fully available on github at [https://github.com/aafagot/GIF\\_OfflineAnalysis](https://github.com/aafagot/GIF_OfflineAnalysis). The software requires ROOT as non-optionnal dependency  
1208 as it takes ROOT files in input and write an output ROOT file containing histograms. To compile the  
1209 GIF++ Offline Analysis project is compiled with cmake. To compile, first a build/ directory must  
1210 be created to compile from there:

```
1212 mkdir build  
1213 cd build  
1214 cmake ..  
1215 make  
1216 make install
```

1214 To clean the directory and create a new build directory, the bash script cleandir.sh can be used:

```
1215  
1216 ./cleandir.sh
```

1217 The source code tree is provided below along with comments to give an overview of the files' con-  
1218 tent. The different objects created for this project (`Infrastructure`, `Trolley`, `RPC`, `Mapping`, `RPCHit`,  
1219 `RPCCluster` and `Inifile`) will be described in details in the following sections.

1220

```

GIF_OfflineAnalysis
├── bin
│   └── offlineanalysis ..... EXECUTABLE
├── build..... CMAKE COMPILATION DIRECTORY
└── ...
    ├── include..... LIST OF C++ HEADER FILES
    │   ├── Cluster.h..... DECLARATION OF OBJECT RPCCLUSTER
    │   ├── Current.h..... DECLARATION OF GETCURRENT ANALYSIS MACRO
    │   ├── GIFTrolley.h..... DECLARATION OF OBJECT TROLLEY
    │   ├── Infrastructure.h..... DECLARATION OF OBJECT INFRASTRUCTURE
    │   ├── IniFile.h..... DECLARATION OF OBJECT INI FILE FORINI PARSER
    │   ├── Mapping.h..... DECLARATION OF OBJECT MAPPING
    │   ├── MsgSvc.h..... DECLARATION OF OFFLINE LOG MESSAGES
    │   ├── OfflineAnalysis.h..... DECLARATION OF DATA ANALYSIS MACRO
    │   ├── RPCTracker.h..... DECLARATION OF OBJECT RPC
    │   ├── RPCHit.h..... DECLARATION OF OBJECT RPCHIT
    │   ├── types.h..... DEFINITION OF USEFUL VARIABLE TYPES
    │   └── utils.h..... DECLARATION OF USEFUL FUNCTIONS
    ├── obj..... BINARY FILES CREATED BY COMPILER
    └── ...
        ├── src..... LIST OF C++ SOURCE FILES
        │   ├── Cluster.cc..... DEFINITION OF OBJECT RPCCLUSTER
        │   ├── Current.cc..... DEFINITION OF GETCURRENT ANALYSIS MACRO
        │   ├── GIFTrolley.cc..... DEFINITION OF OBJECT TROLLEY
        │   ├── Infrastructure.cc..... DEFINITION OF OBJECT INFRASTRUCTURE
        │   ├── IniFile.cc..... DEFINITION OF OBJECT INI FILE FORINI PARSER
        │   ├── main.cc..... MAIN FILE
        │   ├── Mapping.cc..... DEFINITION OF OBJECT MAPPING
        │   ├── MsgSvc.cc..... DEFINITION OF OFFLINE LOG MESSAGES
        │   ├── OfflineAnalysis.cc..... DEFINITION OF DATA ANALYSIS MACRO
        │   ├── RPCTracker.cc..... DEFINITION OF OBJECT RPC
        │   ├── RPCHit.cc..... DEFINITION OF OBJECT RPCHIT
        │   └── utils.cc..... DEFINITION OF USEFUL FUNCTIONS
        ├── cleandir.sh..... BASH SCRIPT TO CLEAN BUILD DIRECTORY
        ├── CMakeLists.txt..... SET OF INSTRUCTIONS FOR CMAKE
        ├── config.h.in..... DEFINITION OF VERSION NUMBER
        └── README.md..... README FILE FOR GITHUB

```

1221

## B.2 Usage of the Offline Analysis

1222

In order to use the Offline Analysis tool, it is necessary to know the Scan number and the HV Step of the run that needs to be analysed. This information needs to be written in the following format:

1224

1225

```
Scan00XXXX_HVY
```

1226

where XXXX is the scan ID and Y is the high voltage step (in case of a high voltage scan, data will be taken for several HV steps). This format corresponds to the base name of data files in the database

1227

1228 of the GIF++ webDCS. Usually, the offline analysis tool is automatically called by the webDCS at  
 1229 the end of data taking or by a user from the webDCS panel if an update of the tool was brought.  
 1230 Nonetheless, an expert can locally launch the analysis for tests on the GIF++ computer, or a user can  
 1231 get the code on its local machine from github and download data from the webDCS for its own anal-  
 1232 ysis. To launch the code, the following command can be used from the `GIF_OfflineAnalysis` folder:

1233  
 1234     `bin/offlineanalysis /path/to/Scan00XXXX_HVY`

1235 where, `/path/to/Scan00XXXX_HVY` refers to the local data files. Then, the offline tool will by itself  
 1236 take care of finding all available ROOT data files present in the folder, as listed below:

- 1237     • `Scan00XXXX_HVY_DAQ.root` containing the TDC data as described in Appendix ?? (events, hit  
 1238       and timestamp lists), and
- 1239     • `Scan00XXXX_HVY_CAEN.root` containing the CAEN mainframe data recorded by the monitor-  
 1240       ing tool webDCS during data taking (HVs and currents of every HV channels). This file is  
 1241       created independently of the DAQ.

## 1242     **B.2.1 Output of the offline tool**

### 1243     **B.2.1.1 ROOT file**

1244 The analysis gives in output ROOT datafiles that are saved into the data folder and called using the  
 1245 naming convention `Scan00XXXX_HVY_Offline.root`. Inside those, a list of `TH1` histograms can be  
 1246 found. Its size will vary as a function of the number of detectors in the setup as each set of histograms  
 1247 is produced detector by detector. For each partition of each chamber, can be found:

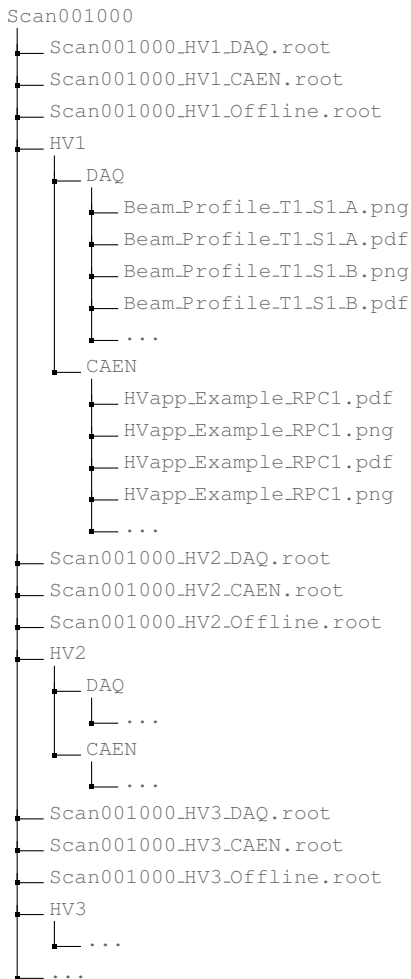
- 1248     • `Time_Profile_Tt_Sc_p` shows the time profile of all recorded events (number of events per  
 1249       time bin),
- 1250     • `Hit_Profile_Tt_Sc_p` shows the hit profile of all recorded events (number of events per chan-  
 1251       nel),
- 1252     • `Hit_Multiplicity_Tt_Sc_p` shows the hit multiplicity (number of hits per event) of all recorded  
 1253       events (number of occurrences per multiplicity bin),
- 1254     • `Strip_Mean_Noise_Tt_Sc_p` shows noise/gamma rate per unit area for each strip in a se-  
 1255       lected time range. After filters are applied on `Time_Profile_Tt_Sc_p`, the filtered version  
 1256       of `Hit_Profile_Tt_Sc_p` is normalised to the total integrated time and active detection area  
 1257       of a single channel,
- 1258     • `Strip_Activity_Tt_Sc_p` shows noise/gamma activity for each strip (normalised version of  
 1259       previous histogram - strip activity = strip rate / average partition rate),
- 1260     • `Strip_Homogeneity_Tt_Sc_p` shows the *homogeneity* of a given partition ( $\text{homogeneity} = \exp(-\text{strip rates standard deviation(strip rates in partition/average partition rate)})$ ),
- 1262     • `mask_Strip_Mean_Noise_Tt_Sc_p` shows noise/gamma rate per unit area for each masked  
 1263       strip in a selected time range. Offline, the user can control the noise/gamma rate and decide to  
 1264       mask the strips that are judged to be noisy or dead. This is done via the *Masking Tool* provided  
 1265       by the webDCS,

- 1266     ● `mask_Strip_Activity_Tt_Sc_p` shows noise/gamma activity per unit area for each masked  
1267       strip with respect to the average rate of active strips,
- 1268     ● `NoiseCSize_H_Tt_Sc_p` shows noise/gamma cluster size, a cluster being constructed out of  
1269       adjacent strips giving a signal at the *same time* (hits within a time window of 25 ns),
- 1270     ● `NoiseCMult_H_Tt_Sc_p` shows noise/gamma cluster multiplicity (number of reconstructed  
1271       clusters per event),
- 1272     ● `Chip_Mean_Noise_Tt_Sc_p` shows the same information than `Strip_Mean_Noise_Tt_Scp` us-  
1273       ing a different binning (1 chip corresponds to 8 strips),
- 1274     ● `Chip_Activity_Tt_Sc_p` shows the same information than `Strip_Activity_Tt_Scp` using  
1275       chip binning,
- 1276     ● `Chip_Homogeneity_Tt_Sc_p` shows the homogeneity of a given partition using chip binning,
- 1277     ● `Beam_Profile_Tt_Sc_p` shows the estimated beam profile when taking efficiency scan. This  
1278       is obtained by filtering `Time_Profile_Tt_Sc_p` to only consider the muon peak where the  
1279       noise/gamma background has been subtracted. The resulting hit profile corresponds to the  
1280       beam profile on the detector channels,
- 1281     ● `L0_Efficiency_Tt_Sc_p` shows the level 0 efficiency that was estimated **without** muon track-  
1282       ing,
- 1283     ● `MuonCSize_H_Tt_Sc_p` shows the level 0 muon cluster size that was estimated **without** muon  
1284       tracking, and
- 1285     ● `MuonCMult_H_Tt_Sc_p` shows the level 0 muon cluster multiplicity that was estimated **without**  
1286       muon tracking.

1287     In the histogram labels,  $t$  stands for the trolley number (1 or 3),  $c$  for the chamber slot label in  
1288     trolley  $t$  and  $p$  for the partition label (A, B, C or D depending on the chamber layout) as explained  
1289     in Chapter 5.3.

1290     In the context of GIF++, an extra script called by the webDCS is called to extract the histograms  
1291     from the ROOT files. The histograms are then stored in PNG and PDF formats into the correspond-  
1292     ing folder (a single folder per HV step, so per ROOT file). the goal is to then display the histograms  
1293     on the Data Quality Monitoring (DQM) page of the webDCS in order for the users to control the  
1294     quality of the data taking at the end of data taking. An example of histogram organisation is given  
1295     below:

1296



**1298      Here can put some screens from the webDCS to show the DQM and the plots available to users.**

**1299**

### **1300      B.2.1.2 CSV files**

**1301      Moreover, up to 3 CSV files can be created depending on which ones of the 3 input files were in the**

**1302      data folder:**

- 1303      • Offline-Rate.csv : contains the summary of the noise/gamma hit and cluster rates for each**
- 1304      chamber partitions,**
- 1305      • Offline-Current.csv : contains the summary of the currents and voltages applied on each**
- 1306      RPC HV channel, and**
- 1307      • Offline-L0-EffCl.csv : contains the summary of the level 0 efficiency and muon cluster**
- 1308      information **without** tracking.**

**1309      Note that these 3 CSV files are created along with their *headers* (*offline-[...]-Header.csv***

**1310      containing the names of each data columns) and are automatically merged together when the offline**

1311 analysis tool is called from the webDCS, contrary to the case where the tool is runned locally from  
 1312 the terminal as the merging bash script is then not called. Thus, the resulting files, used to make  
 1313 official plots, are:

- 1314     ● Rate.csv ,
- 1315     ● Current.csv ,
- 1316     ● L0-EffCl.csv .

## 1317     **B.3 Analysis inputs and information handling**

1318 The usage of the Offline Analysis tool as well as its output have been presented in the previous sec-  
 1319 tion. It is now important to dig further and start looking at the source code and the inputs necessary  
 1320 for the tool to work. Indeed, other than the raw ROOT data files that are analysed, more information  
 1321 needs to be imported inside of the program to perform the analysis such as the description of the  
 1322 setup inside of GIF++ at the time of data taking (number of trolleys, of RPCs, dimensions of the  
 1323 detectors, etc...) or the mapping that links the TDC channels to the coresponding RPC channels in  
 1324 order to translate the TDC information into human readable data. 2 files are used to transmit all this  
 1325 information:

1326

- 1327     ● Dimensions.ini, that provides the necessary setup and RPC information, and
- 1328     ● ChannelsMapping.csv, that gives the link between the TDC and RPC channels as well as the  
       *mask* for each channel (masked or not?).

### 1330     **B.3.1 Dimensions file and IniFile parser**

1331 This input file, present in every data folder, allows the analysis tool to know of the number of ac-  
 1332 tive trolleys, the number of active RPCs in those trolleys, and the details about each RPCs such as  
 1333 the number of RPC gaps, the number of pseudo-rapidity partitions (for CMS-like prototypes), the  
 1334 number of strips per partion or the dimensions. To do so, there are 3 types of groups in the INI file  
 1335 architecture. A first general group, appearing only once at the head of the document, gives informa-  
 1336 tion about the number of active trolleys as well as their IDs, as presented in Source Code B.1. For  
 1337 each active trolley, a group similar to Source Code B.2 can be found containing information about  
 1338 the number of active detectors in the trolley and their IDs. Each trolley group as a `Tt` name format,  
 1339 where `t` is the trolley ID. Finally, for each detector stored in slots of an active trolley, there is a group  
 1340 providing information about their names and dimensions, as showed in Source Code B.3. Each slot  
 1341 group as a `TtSs` name format, where `s` is the slot ID of trolley `t` where the active RPC is hosted.

1342

```
[General]
nTrolleys=2
TrolleysID=13
```

1344 *Source Code B.1: Example of [General] group as might be found in Dimensions.ini. In GIF++, only 2  
 trolleys are available to hold RPCs and place them inside of the bunker for irradiation. The IDs of the trolleys  
 are written in a signle string as "13" and then read character by character by the program.*

```
1345 [T1]
nSlots=4
SlotsID=1234
```

Source Code B.2: Example of trolley group as might be found in `Dimensions.ini`. In this example, the file tells that there are 4 detectors placed in the holding slots of the trolley T1 and that their IDs, written as a single string variable, are 1, 2, 3 and 4.

```
1346 [T1S1]
Name=RE2-2-NPD-BARC-8
Partitions=3
Gaps=3
Gap1=BOT
Gap2=TN
Gap3=TW
AreaGap1=11694.25
AreaGap2=6432
AreaGap3=4582.82
Strips=32
ActiveArea-A=157.8
ActiveArea-B=121.69
ActiveArea-C=93.03
```

Source Code B.3: Example of slot group as might be found in `Dimensions.ini`. In this example, the file provides information about a detector named RE2-2-NPD-BARC-8, having 3 pseudo-rapidity readout partitions and stored in slot S1 of trolley T1. This is a CMS RE2-2 type of detector. This information will then be used for example to compute the rate per unit area calculation.

This information is readout and stored in a C++ object called `IniFile`, that parses the information in the INI input file and stores it into a local buffer for later use. This INI parser is the exact same one that was previously developed for the GIFT++ DAQ and described in Appendix A.5.2.

### 1352 B.3.2 TDC to RPC link file and Mapping

1353 The same way the INI dimension file information is stored using `map`, the channel mapping and mask  
 1354 information is stored and accessed through `map`. First of all, the mapping CSV file is organised into  
 1355 3 columns separated by tabulations (and not by commas, as expected for CSV files as it is easier using  
 1356 streams to read tab or space separated data using C++):

```
1357
1358   RPC_channel      TDC_channel      mask
```

1359 using as formatting for each field:

```
1360
1361   TSCCC      TCCC      M
```

1362 `TSCCC` is a 5-digit integer where `T` is the trolley ID, `s` the slot ID in which the RPC is held insite  
 1363 the trolley `T` and `ccc` is the RPC channel number, or *strip* number, that can take values up to  
 1364 3-digits depending on the detector,

1365 `TCCC` is a 4 digit integer where `T` is the TDC ID, `ccc` is the TDC channel number that can take values  
 1366 in between 0 and 127, and

1367     M is a 1-digit integer indicating if the channel should be considered (M = 1) or discarded (M = 0)  
 1368     during analysis.

1369     This mapping and masking information is readout and stored thanks to the object `Mapping`, pre-  
 1370     sented in Source Code B.4. Similarly to `IniFile` objects, this class has private methods. The first  
 1371     one, `Mapping::CheckIfNewLine()` is used to find the newline character '`\n`' or return character  
 1372     '`\r`' (depending on which kind of operating system interacted with the file). This is used for the  
 1373     simple reason that the masking information has been introduced only during the year 2017 but the  
 1374     channel mapping files exist since 2015 and the very beginning of data taking at GIFT++. This means  
 1375     that in the older data folders, before the upgrade, the channel mapping file only had 2 columns, the  
 1376     RPC channel and the TDC channel. For compatibility reasons, this method helps controlling the  
 1377     character following the readout of the 2 first fields of a line. In case any end of line character is  
 1378     found, no mask information is present in the file and the default M = 1 is used. On the contrary, if  
 1379     the next character was a tabulation or a space, the mask information is present.

1380     Once the 3 fields have been readout, the second private method `Mapping::CheckIfTDCCh()` is  
 1381     used to control that the TDC channel is an existing TDC channel. Finally, the information is stored  
 1382     into 3 different maps (`Link`, `ReverseLink` and `Mask`) thanks to the public method `Mapping::Read()`.  
 1383     `Link` allows to get the RPC channel by knowing the TDC channel while `ReverseLink` does the op-  
 1384     posite by returning the TDC channel by knowing the RPC channel. Finally, `Mask` returns the mask  
 1385     associated to a given RPC channel.

```
1386
typedef map<UInt, UInt> MappingData;

class Mapping {
  private:
    bool          CheckIfNewLine(char next);
    bool          CheckIfTDCCh(UInt channel);
    string        FileName;
    MappingData Link;
    MappingData ReverseLink;
    MappingData Mask;
    int           Error;

1387
  public:
    Mapping();
    Mapping(string baseName);
    ~Mapping();

    void SetFileName(const string filename);
    int  Read();
    UInt GetLink(UInt tdcchannel);
    UInt GetReverse(UInt rpcchannel);
    UInt GetMask(UInt rpcchannel);
};
```

1388     Source Code B.4: Description of C++ object `Mapping` used as a parser for the channel mapping and mask file.

## 1389     B.4 Description of GIFT++ setup within the Offline Analysis tool

1390     In the previous section, the tool input files have been discussed. The dimension file information is  
 1391     stored in a map hosted by the `IniFile` object. But this information is then used to create a series of

1392 new objects that helps defining the Gif++ infrastructure directly into the Offline Analysis. Indeed,  
 1393 from the `RPC`, to the more general `Infrastructure`, every element of the Gif++ infrastrucutre is  
 1394 recreated for each data analysis based on the information provided in input. All this information  
 1395 about the infrastructure will be used to assign each hit signal to a specific strip channel of a specific  
 1396 detector, and having a specific active area. This way, rate per unit area calculation is possible.

1397

### 1398 B.4.1 RPC objects

1399 `RPC` objects have been developped to represent physical active detectors in Gif++ at the moment  
 1400 of data taking. Thus, there are as many `RPC` objects created during the analysis than there were  
 1401 active RPCs tested during a run. Each `RPC` hosts the information present in the corresponding INI  
 1402 slot group, as shown in B.3, and organises it using a similar architecture. This can be seen from  
 1403 Source Code B.5.

1404 To make the object more compact, the lists of gap labels, of gap active areas and strip active  
 1405 areas are stored into `vector` dynamical containers. `RPC` objects are always contructed thanks to the  
 1406 dimension file information stored into the `IniFILE` and their ID, using the format `TtSs`. Using the  
 1407 `RPC` ID, the constructor calls the methods of `IniFile` to initialise the `RPC`. The other constructors  
 1408 are not used but exist in case of need. Finally, some getters have been written to access the different  
 1409 private parameters storing the detector information.

1410

```
1411 class RPC{
1412     private:
1413         string           name;          //RPC name as in webDCS database
1414         Uint             nGaps;        //Number of gaps in the RPC
1415         Uint             nPartitions; //Number of partitions in the RPC
1416         Uint             nStrips;      //Number of strips per partition
1417         vector<string> gaps;        //List of gap labels (BOT, TOP, etc...)
1418         vector<float>    gapGeo;       //List of gap active areas
1419         vector<float>    stripGeo;     //List of strip active areas
1420
1421     public:
1422         RPC();
1423         RPC(string ID, IniFile* geofile);
1424         RPC(const RPC& other);
1425         ~RPC();
1426         RPC& operator=(const RPC& other);
1427
1428         string GetName();
1429         Uint   GetNGaps();
1430         Uint   GetNPartitions();
1431         Uint   GetNStrips();
1432         string GetGap(Uint g);
1433         float  GetGapGeo(Uint g);
1434         float  GetStripGeo(Uint p);
1435     };

```

1412 *Source Code B.5: Description of C++ objects `RPC` that describe each active detectors used during data taking.*

### 1413 B.4.2 Trolley objects

1414 `Trolley` objects have been developped to represent physical active trolleys in Gif++ at the moment

1415 of data taking. Thus, there are as many trolley objects created during the analysis than there were  
 1416 active trolleys hosting tested RPCs during a run. Each `Trolley` hosts the information present in the  
 1417 corresponding INI trolley group, as shown in B.2, and organises it using a similar architecture. In  
 1418 addition to the information hosted in the INI file, these object have a dynamical container of `RPC`  
 1419 objects, representing the active detectors the active trolley was hosting at the time of data taking.  
 1420 This can been seen from Source Code B.6.

1421 `Trolley` objects are always contructed thanks to the dimension file information stored into the  
 1422 `IniFILE` and their ID, using the format `Tt`. Using the Trolley ID, the constructor calls the methods  
 1423 of `IniFile` to initialise the `Trolley`. Retrieving the information of the RPC IDs via `SlotsID`, a new  
 1424 `RPC` is constructed and added to the container `RPCs` for each character in the ID string. The other  
 1425 constructors are not used but exist in case of need. Finally, some getters have been written to access  
 1426 the different private parameters storing the trolley and detectors information.

1427

```
class Trolley{
    private:
        Uint      nSlots; //Number of active RPCs in the considered trolley
        string   SlotsID; //Active RPC IDs written into a string
        vector<RPC*> RPCs; //List of active RPCs

    public:
        //Constructors, destructor and operator =
        Trolley();
        Trolley(string ID, IniFile* geofile);
        Trolley(const Trolley& other);
        ~Trolley();
        Trolley& operator=(const Trolley& other);

        //Get GIFTrolley members
        Uint   GetNSlots();
        string GetSlotsID();
        Uint   GetSlotID(Uint s);

        //Manage RPC list
        RPC*   GetRPC(Uint r);
        void   DeleteRPC(Uint r);

        //Methods to get members of RPC objects stored in RPCs
        string GetName(Uint r);
        Uint   GetNGaps(Uint r);
        Uint   GetNPartitions(Uint r);
        Uint   GetNStrips(Uint r);
        string GetGap(Uint r, Uint g);
        float  GetGapGeo(Uint r, Uint g);
        float  GetStripGeo(Uint r, Uint p);
};
```

1429 *Source Code B.6: Description of C++ objects `Trolley` that describe each active trolley used during data  
 taking.*

### 1430 B.4.3 Infrastructure object

1431 The `Infrastructure` object has been developped to represent the GIFT++ bunker area dedicated to  
 1432 CMS RPC experiments. With this very specific object, all the information about the CMS RPC  
 1433 setup within GIFT++ at the moment of data taking is stored. It hosts the information present in the

1434 corresponding INI general group, as shown in B.1, and organises it using a similar architecture. In  
 1435 addition to the information hosted in the INI file, this object have a dynamical container of `Trolley`  
 1436 objects, representing the active tolleys in GIFT++ area. This can been seen from Source Code B.7.

1437 The `Infrastructure` object is always contructed thanks to the dimension file information stored  
 1438 into the `IniFILE`. Retrieving the information of the trolley IDs via `TrolleysID`, a new `Trolley` is  
 1439 constructed and added to the container `Trolleys` for each character in the ID string. By extension,  
 1440 it is easy to understand that the process described in Section B.4.2 for the construction of RPCs  
 1441 takes place when a trolley is constructed. The other constructors are not used but exist in case of  
 1442 need. Finally, some getters have been written to access the different private parameters storing the  
 1443 infrastructure, tolleys and detectors information.

```
1444
1445   class Infrastructure {
1446     private:
1447       Uint           nTrolleys; //Number of active Trolleys in the run
1448       string         TrolleysID; //Active trolley IDs written into a string
1449       vector<Trolley*> Trolleys; //List of active Trolleys (struct)
1450
1451     public:
1452       //Constructors and destructor
1453       Infrastructure();
1454       Infrastructure(IniFile* geofile);
1455       Infrastructure(const Infrastructure& other);
1456       ~Infrastructure();
1457       Infrastructure& operator=(const Infrastructure& other);
1458
1459       //Get Infrastructure members
1460       Uint   GetNTrolleys();
1461       string GetTrolleysID();
1462       Uint   GetTrolleyID(Uint t);
1463
1464       //Manage Trolleys
1465       Trolley* GetTrolley(Uint t);
1466       void    DeleteTrolley(Uint t);
1467
1468       //Methods to get members of GIFTrolley objects stored in Trolleys
1469       Uint   GetNSlots(Uint t);
1470       string GetSlotsID(Uint t);
1471       Uint   GetSlotID(Uint t, Uint s);
1472       RPC*  GetRPC(Uint t, Uint r);
1473
1474       //Methods to get members of RPC objects stored in RPCs
1475       string GetName(Uint t, Uint r);
1476       Uint   GetNGaps(Uint t, Uint r);
1477       Uint   GetNPartitions(Uint t, Uint r);
1478       Uint   GetNStrips(Uint t, Uint r);
1479       string GetGap(Uint t, Uint r, Uint g);
1480       float  GetGapGeo(Uint t, Uint r, Uint g);
1481       float  GetStripGeo(Uint t, Uint r, Uint p);
1482   };

```

1446 *Source Code B.7: Description of C++ object `Infrastructure` that contains the full information about CMS  
 RPC experiment in GIFT++.*

## 1447 B.5 Handeling of data

1448 As discussed in Appendix A.4.2, the raw data as a `TTree` architecture where every entry is related to  
 1449 a trigger signal provided by a muon or a random pulse, whether the goal of the data taking was to  
 1450 measure the performance of the detector or the noise/gamma background respectively. Each of these  
 1451 entries, referred also as events, contain a more or less full list of hits in the TDC channels to which  
 1452 the detectors are connected. To this list of hits corresponds a list of time stamps, marking the arrival  
 1453 of the hits within the TDC channel.

1454 The infrastructure of the CMS RPC experiment within `GIF++` being defined, combining the  
 1455 information about the raw data with the information provided by both the mapping/mask file and the  
 1456 dimension file allows to build new physical objects that will help in computing efficiency or rates.

### 1457 B.5.1 RPC hits

1458 The raw data stored in the ROOT file as output of the `GIF++` DAQ, is readout by the analysis tool  
 1459 using the structure `RAWData` presented in Source Code B.9 that differs from the structure presented  
 1460 in Appendix A.4.2 as it is not meant to hold all of the data contained in the ROOT file. In this sense,  
 1461 this structure is in the case of the offline analysis tool not a dynamical object and will only be storing  
 1462 a single event contained in a single entry of the `TTree`.

```
1463
1464 class RPCHit {
1465     private:
1466     Uint Channel;      //RPC channel according to mapping (5 digits)
1467     Uint Trolley;       //0, 1 or 3 (1st digit of the RPC channel)
1468     Uint Station;       //Slot where is held the RPC in Trolley (2nd digit)
1469     Uint Strip;         //Physical RPC strip where the hit occured (last 3
1470     → digits)
1471     Uint Partition;    //Readout partition along eta segmentation
1472     float TimeStamp;   //Time stamp of the arrival in TDC
1473
1474     public:
1475     //Constructors, destructor & operator =
1476     RPCHit();
1477     RPCHit(Uint channel, float time, Infrastructure* Infra);
1478     RPCHit(const RPCHit& other);
1479     ~RPCHit();
1480     RPCHit& operator=(const RPCHit& other);
1481
1482     //Get RPCHit members
1483     Uint GetChannel();
1484     Uint GetTrolley();
1485     Uint GetStation();
1486     Uint GetStrip();
1487     Uint GetPartition();
1488     float GetTime();
1489 };
1490
1491 typedef vector<RPCHit> HitList;
1492 typedef struct GIFHitList { HitList rpc[NTROLLEYS][NSLOTS][NPARTITIONS]; } → GIFHitList;
1493
1494 bool SortHitbyStrip(RPCHit h1, RPCHit h2);
1495 bool SortHitbyTime(RPCHit h1, RPCHit h2);
```

```

1466 struct RAWData{
1467     int iEvent;      //Event i
1468     int TDCNHits;   //Number of hits in event i
1469     int QFlag;      //Quality flag list (1 flag digit per TDC)
1470     vector<UInt> *TDCCh;    //List of channels giving hits per event
1471     vector<float> *TDCTS;    //List of the corresponding time stamps
1472 };

```

1467                  *Source Code B.9: Description of C++ structure RAWData.*

1468     Each member of the structure is then linked to the corresponding branch of the ROOT data tree,  
1469     as shown in the example of Source Code B.10, and using the method `GetEntry(int i)` of the ROOT  
1470     class `TTree` will update the state of the members of `RAWData`.

```

1471 TTree* dataTree = (TTree*)dataFile.Get("RAWData");
1472 RAWData data;
1473
1474 dataTree->SetBranchAddress("EventNumber", &data.iEvent);
1475 dataTree->SetBranchAddress("number_of_hits", &data.TDCNHits);
1476 dataTree->SetBranchAddress("Quality_flag", &data.QFlag);
1477 dataTree->SetBranchAddress("TDC_channel", &data.TDCCh);
1478 dataTree->SetBranchAddress("TDC_TimeStamp", &data.TDCTS);

```

1473                  *Source Code B.10: Example of link in between RAWData and TTree.*

1474     The data is then analysed entry by entry and to each element of the TDC channel list, a `RPCHit` is  
1475     constructed by linking each TDC channel to the corresponding RPC channel thanks to the `Mapping`  
1476     object. The information carried by the RPC channel format allows to easily retrieve the trolley and  
1477     slot from which the hit was recorded (see section B.3.2). Using these 2 values, the readout partition  
1478     can be found by knowing the strip channel and comparing it with the number of partitions and strips  
1479     per partition stored into the `Infrastructure` object.

1480     Thus `RPCHit` objects are then stored into 3D dynamical list called `GIFHitList` (Source Code B.9)  
1481     where the 3 dimensions refer to the 3 layers of the readout in `GIF++` : in the bunker there are *trolleys*  
1482     ( $\tau$ ) holding detectors in *slots* ( $s$ ) and each detector readout is divided into 1 or more pseudo-rapidity  
1483     *partitions* ( $p$ ). Using these 3 information allows to assign an address to each readout partition and  
1484     this address will point to a specific hit list.

1485

## 1486     **B.5.2 Clusters of hits**

1487     All the hits contained in the ROOT file have been sorted into the different hit lists through the  
1488     `GIFHitList`. At this point, it is possible to start looking for clusters. A cluster is a group of adjacent  
1489     strips getting hits within a time window of 25 ns. These strips are then assumed to be part of the same  
1490     physical avalanche signal generated by a muon passing through the chamber or by the interaction of  
1491     a gamma stopping into the electrodes of the RPCs.

1492     To keep the cluster information, `RPCCluster` objects have been defined as shown in Source  
1493     Code B.11. Using the information of each individual `RPCHit` taken out of the hit list, it stores  
1494     the cluster size (number of adjacent strips composing the cluster), the first and last hit, the center for  
1495     spatial reconstruction and finally the start and stop time stamps as well as te time spread in between

1496 the first and last hit.

1497

```

class RPCCluster{
    private:
        Uint ClusterSize; //Size of cluster #ID
        Uint FirstStrip; //First strip of cluster #ID
        Uint LastStrip; //Last strip of cluster #ID
        float Center; //Center of cluster #ID ((first+last)/2)
        float StartStamp; //Time stamp of the earliest hit of cluster #ID
        float StopStamp; //Time stamp of the latest hit of cluster #ID
        float TimeSpread; //Time difference between earliest and latest hits
                           //of cluster #ID
    public:
        //Constructors, destructor & operator =
        RPCCluster();
        RPCCluster(HitList List, Uint cID, Uint cSize, Uint first, Uint firstID);
        RPCCluster(const RPCCluster& other);
        ~RPCCluster();
        RPCCluster& operator=(const RPCCluster& other);

        //Get Cluster members
        Uint GetID();
        Uint GetSize();
        Uint GetFirstStrip();
        Uint GetLastStrip();
        float GetCenter();
        float GetStart();
        float GetStop();
        float GetSpread();
    };

    typedef vector<RPCCluster> ClusterList;

    //Other functions to build cluster lists out of hit lists
    void BuildClusters(HitList &cluster, ClusterList &clusterList);
    void Clusterization(HitList &hits, TH1 *hcSize, TH1 *hcMult);
}

```

1498

1499

*Source Code B.11: Description of C++ object Cluster.*

1500

To investigate the hit list of a given detector partition, the function `Clusterization()` defined in `include/Cluster.h` needs the hits in the list to be time sorted. This is achieved by calling function `sort()` of library `<algorithm>` using the comparator `SortHitbyTime(RPCHit h1, RPCHit h2)` defined in `include/RPCHit.h` that returns `true` if the time stamp of hit `h1` is lower than that of `h2`. A first isolation of strips is made only based on time information. All the hits within the 25 ns window are taken separately from the rest. Then, this sub-list of hits is sorted this time by ascending strip number, using this time the comparator `SortHitbyStrip(RPCHit h1, RPCHit h2)`. Finally, the groups of adjacent strips are used to construct `RPCCluster` objects that are then stored in a temporary list of clusters that is at the end of the process used to know how many clusters were reconstructed and to fill their sizes into an histogram that will allows to know the mean size of muon or gamma clusters.

1501

1502

1503

1504

1505

1506

1507

1508

1509

1510

1511

# C

1512

1513

## Structure of the hybrid simulation software

1514

### C.1 Introduction

1515

insert text here...

